Journal of Materials Chemistry A

REVIEW

View Article Online
View Journal | View Issue

Cite this: J. Mater. Chem. A, 2022, 10, 2672

Regioregularity-control of conjugated polymers: from synthesis and properties, to photovoltaic device applications

Youngkwon Kim, †[a] Hyeonjung Park, †[a] Jin Su Park,[a] Jin-Woo Lee,[a] Felix Sunjoo Kim, [d] Hyeong Jun Kim *[c] and Bumjoon J. Kim *[ab]

Received 30th September 2021
Accepted 22nd December 2021

DOI: 10.1039/d1ta08495j

rsc.li/materials-a

In the last few decades, extensive academic and industrial efforts have been devoted to developing high-performance conjugated polymers (CPs) for organic electronics. Specifically, the relationships between the molecular structures of CPs and their properties and device characteristics have been a subject of intense studies. In this review, we highlight recent advances in the molecular design of CPs, particularly on tuning their regioregularity (RR). The RR of repeating units (*i.e.*, directional, positional, and sequential regularities) within the CP backbone determines the intrinsic properties of CPs and the performances of the resulting devices. Despite the significant impact of RR on the overall properties of the polymers and the device performances, the importance of RR in the design of CPs has yet to be emphasized. Furthermore, RR control is critical in state-of-the-art CPs with asymmetric molecular structures. This review presents a library of examples that report the impact of RR control in CPs on the properties and performances in various organic electronic devices, including simple homopolymers with asymmetric alkyl side chains and more recently developed copolymers with various donor–acceptor (D–A) combinations. This review summarizes important guidelines and provides insights for the molecular design of RR-controlled CPs and their applications in efficient organic electronics.

1. Introduction

The development of high-performance conjugated polymers (CPs) has been a long-sought goal for numerous organic electronic applications such as polymer solar cells (PSCs), organic light-emitting diodes (OLEDs), and organic field-effect transistors (OFETs).[1–7] Through a proper design with versatile chemical structures, CPs can afford excellent optoelectrical and

[a]Department of Chemical and Biomolecular Engineering, Korea Advanced Institute of Science and Technology (KAIST), Daejeon 34141, Republic of Korea. E-mail: bumjoonkim@kaist.ac.kr

[b]KAIST Institute for the Nanocentury, Korea Advanced Institute of Science and Technology (KAIST), Daejeon 34141, Republic of Korea

[c]Department of Chemical and Biomolecular Engineering, Sogang University, Seoul 04107, Republic of Korea. E-mail: hjunkim@sogang.ac.kr

[d]School of Chemical Engineering and Materials Science, Chung-Ang University, Seoul, 06974, Republic of Korea

† Y. Kim and H. Park contributed equally to this work.

Youngkwon Kim received a B.S. degree from the Department of Chemical and Biomolecular Engineering from KAIST in 2014 and a Ph.D. degree under Prof. Bumjoon Kim from KAIST in 2020. Afterward he joined Samsung Electronics as a staff engineer. His research focuses on synthesizing functional conjugated polymers, conjugated polymer-based block copolymer self-assembly, and organic electronic applications.

Hyeonjung Park received a B.S. degree from the Department of Chemical and Biomolecular Engineering from KAIST in 2016. She is currently a Ph.D. candidate under Prof. Bumjoon Kim in KAIST. Her research focuses on the development of high-performance and functional conjugated polymers for organic electronics and mechanical/crystallization behaviors of conjugated polymers.

mechanical properties and solution processability for cost-effective production.[8–10] These unique features have driven a significant amount of academic and industrial efforts to develop an extensive library of CPs. From these efforts, the figures of merit of organic electronic devices employing CPs have been improved to approach the benchmarks for commercialization typically achieved with electronic devices based on inorganic semiconductors.

With the successful demonstration of CP-based devices, several important molecular design guidelines have been established. These include the backbone structure, alkyl side chain selection, electron-rich donor (D)–electron-poor acceptor (A) alternating copolymer structures, and various electron-withdrawing/donating moieties for efficient CPs.[11–14] The impact of the molecular structures of CPs on their optoelectrical properties and corresponding device performances has been extensively investigated.[15–18] Among many molecular design parameters, the regioregularity (RR)—geometric regularity of repeating units in CPs—has emerged as an important criterion for achieving high-performance CPs with complex chemical structures.[19–21] Although previous literature has revealed the impact of RR on the properties of CPs and the associated device performances,[22–26] the importance of RR in the design of CPs has attracted less attention.

In this review, we describe RR control in a variety of CPs and overview its impact on the properties of CPs and their performances in photovoltaic devices, including recent examples of the state-of-the-art D–A copolymers. Traditionally, the definition of RR has been limited to simple homopolymers with asymmetric alkyl side chains such as poly(3-alkylthiophene)s (P3ATs). To expand our understanding of RR to more sophisticated CP structures, three different categories of RRs are considered: (i) directional RR, (ii) positional RR, and (iii) sequential RR. While several reports independently define the RR of different CPs including D–A copolymers, the more systematic classification of RR introduced in this review will improve our understanding of the structure of CPs in terms of their RR. This review presents a library of examples of directional, positional, and sequential RR-controlled CPs and summarizes the impact of RR on the properties of CPs and their performances in organic electronics. Finally, the conclusions drawn from this review and the outlook for further development of RR-controlled CPs are presented.

2. Regioregularity of conjugated polymers

2.1. Definition of regioregularity (RR)

The RR of CPs describes the geometrical symmetry of each monomer unit along the polymer chain. The number of identical regio-isomers in the polymers determines RR, *i.e.*, a RR of 100% indicates perfectly regio-regular (*rre*) CPs, where all repeating units in the polymers consist of the same regio-isomer. Thus, the presence of other regio-isomers lowers the RR of the CPs. The RR of polymeric materials, particularly of CPs, strongly impacts their intrinsic properties such as thermal, crystalline, rheological, mechanical and optoelectrical properties. The definition of RR of CPs has been well-established for simple conjugated homopolymers with asymmetric alkyl side chains.[20,21] However, a more systematic definition of RR is required for state-of-the-art CPs with more complex chemical structures. While several excellent research papers and reviews independently define RR of advanced conjugated materials,[19–21] this review presents an extensive library of recent high-performance CPs and classifies them into three categories: directional RR; positional RR; and sequential RR (Fig. 1).

Directional RR is defined as the fraction of asymmetric repeating units that are arranged in the same direction along a polymer chain. The most representative example of directional RR is P3ATs. During the polymerization of P3ATs, two 3-alkylthiophenes can adopt four possible arrangements: head-to-head (H–H), tail-to-tail (T–T), and two head-to-tail (H–T) bonded thiophene rings. In these systems, the RR of P3ATs is quantified by the amount of H–T bonds in the polymer chain.[27–29] Perfectly *rre* P3AT

Hyeong Jun Kim is an assistant professor in the Department of Chemical and Biomolecular Engineering at Sogang University. He received a Ph.D degree from the Department of Chemical and Biomolecular Engineering at KAIST under the supervision of prof. Bumjoon Kim. After that, He joined the University of Massachusetts Amherst in the Department of Polymer Science and engineering as a postdoctoral research associate. His postdoc host was prof. Ryan Hayward. His research interests involve physical phenomena of charged and conjugated macromolecules as well as their applications in soft ionic/electronic devices.

Bumjoon Kim is a KAIST Endowed Chair Professor and Department Head of the Department of Chemical and Biomolecular Engineering at KAIST. He received his Ph.D. degree from UC Santa Barbara under the guidance of Prof. Edward Kramer. Afterward he worked with Prof. Jean Fréchet at UC Berkeley as a postdoc researcher. His current research includes polymer designs for the development of high-performance and mechanically-robust solar cells, polymeric electrolyte and smart responsive block copolymer-based particles.

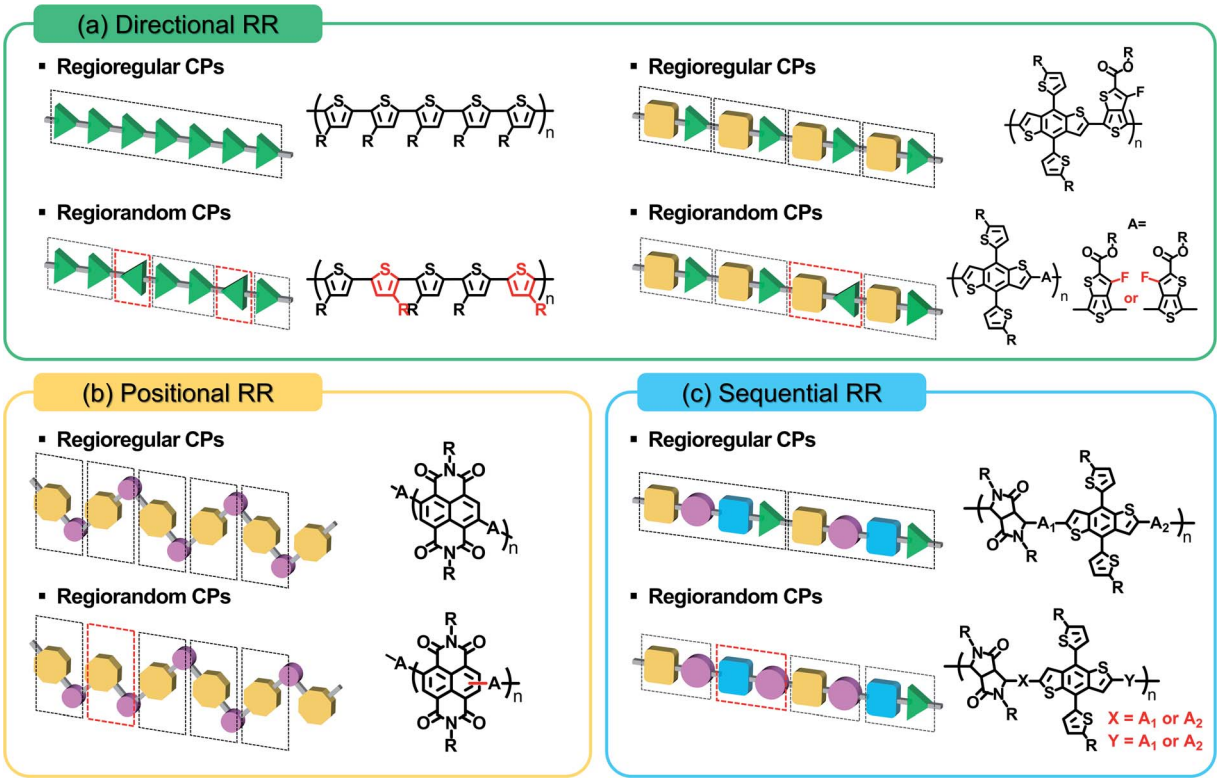

Fig. 1 Structural representation of (a) directional, (b) positional, and (c) sequential RRs of CPs.

contains solely H–T bonds whereas the regio-random (*rra*) one comprises a mixture of isomers, resulting in randomly oriented alkyl chains along the CP backbone (RR = 50%). Similarly, directional RR in other types of CPs can be determined by the directional orientation of the functional groups or side-chains along the conjugated backbone.[30–35] One example of D–A type CPs with directional RR is poly[4,8-bis(5-(2-ethylhexyl)thiophene-2-yl)benzo[1,2-*b*:4,5-*b*′]dithiophene-2,6-diyl-*alt*-(4-(2-ethylhexyl)-3-fluorothieno[3,4-*b*]thiophene-)-2-carboxylate-2-6-diyl] (PTB7-Th), where D is a symmetric benzodithiophene and A is an asymmetric fluoro-substituted thienothiophene (Fig. 1a).[36] *rre* PTB7-Th can be obtained when the fluorine moieties are arranged in one direction along the polymer backbone, whereas *rra* PTB7-Th contains randomly oriented fluorine atoms along the chain.

RR can also be represented by the positional orientation of covalent bonds between monomer units in CP backbones.[37–42] An example of positional RR can be found in poly([*N*,*N*′-bis(2-octyldodecyl)naphthalene-1,4,5,8-bis(dicarboximide)-2,6-diyl]-*alt*-5,5′-(2,2′-bithiophene)) (P(NDI2OD-T2) or N2200), which is one of the most widely used n-type CPs.[42–44] The naphthalene diimide (NDI) repeating moiety of P(NDI2OD-T2) has four different reactive sites for hydrogen, which can be substituted with bromines in the 2,6- or 2,7-position. Then, the mixture of brominated NDI monomers can undergo either 2,6- or 2,7-oxidation additions between the D and A units during polymerization, resulting in positional regio-isomers (Fig. 1b). Thus, positional RR is defined by the number of the same additions included in the P(NDI2OD-T2) polymer chains. *rre* P(NDI2OD-T2) has one type of addition (either 2,6 or 2,7) of NDI, whereas *rra* P(NDI2OD-T2) contains a random mixture of isomerized bonds. Similarly, positional RR can be defined for other CPs if the constituent monomers contain more than one active polymerization site.

Lastly, many D–A alternating copolymers can exhibit sequential RR.[45–50] Most of the recent high-performance CPs used in organic electronics are based on D–A molecular structures, where D and A are alternately coupled along the CP backbones. In general, D–A copolymers are prepared *via* multiple coupling reactions between D and A moieties in an alternating sequence of D–A structures. When the molecular structure of D or A is asymmetric, sequential regularity—H–H or H–T arrangements—can be induced during the coupling polymerization (Fig. 1c). Moreover, different monomer sequences can be introduced in conjugated terpolymers (D–A1–D–A2) or tetrapolymers (D1–A1–D2–A2).[45–49] Sequentially *rre* terpolymers or tetrapolymers comprise repeating (D1–A1) and (D2–A2) sequences (or (D–A1) and (D–A2)) that alternate throughout the polymer chain. In contrast, *rra* polymers comprise a random sequence of donors (D1 or D2) and acceptors (A1 or A2) in the conjugated terpolymers or tetrapolymers.

Here, we present an overview of directional, positional and sequential RR controlled CPs and their intrinsic properties, starting from simple conjugated homopolymers with asymmetric alkyl chains. Thereafter, the discussion is expanded to more recently developed complex CP structures, particularly focusing on the D–A type copolymers.

2.2 RR control of homopolymers with asymmetric alkyl chains

In the early 1970s, P3ATs were developed by incorporating alkyl side chains along the thiophene backbone to address the low solution processability of polythiophenes.[51–53] During that time, P3ATs were often obtained by the reduction of thiophene rings from electro-chemical polymerization with strong dopants such as $FeCl_3$, $LiBF_4$, and NBu_4PF_6 (**A–D**).[54–56] Although these methods offer a facile synthesis of P3ATs, most electro-chemical methods typically yield regio-irregular (*rir*) P3ATs as regio-selective coupling of 3-alkylthiophenes does not occur during the electro-chemical polymerization process. We note that *rra* indicates nearly 50% of RR, while *rir* indicates the middle range of RR between *rre* and *rra* (*e.g.*, RR = 80 and 70%, Fig. 2).

A *rre* P3AT was first synthesized by McCullough in 1992 using lithium diisopropylamide and $MgBr_2 \cdot Et_2O$ with 2-bromo-3-alkylthiophene to produce 2-bromo-5-bromomagnesio-3-alkylthiophene for regio-selective coupling of 3-alkylthiophenes.[57–59] Subsequent catalyst transfer polymerization (CTP) of 2-bromo-5-bromomagnesio-3-alkylthiophene by a cross-coupling reaction in the presence of a Ni(dppp)Cl_2 catalyst afforded the target with 98–100% of RR (**E**).[60] Around the same time, the Rieke method was developed, where 2,5-dibromo-3-alkylthiophenes react with Rieke Zn and are subsequently polymerized with Ni(dppe)Cl_2 to yield high RR (≥97%) P3ATs (**F**). Different degrees of RR can be achieved by employing different organic ligands and metal catalysts.[61,62] For example, RRs of 70%, 65%, and 50% were obtained by CTP using Pd(dppe)Cl_2, Ni(PPh_3)$_4$, and Pd(PPh_3)$_4$ catalysts, respectively (**G–I**). In 1999, McCullough developed Grignard metathesis (GRIM method) with alkyl-MgCl to provide regio-selectivity for 2,5-dibromo-3-alkylthiophenes without cryogenic temperatures and hazardous metal catalysts (**J**).[63] Importantly, the CTP method can exhibit a living behavior, with precise control of the molecular weight and narrow dispersity, making it an attractive model system for investigating the fundamentals of CPs, including their molecular behaviors and properties.[64–67] Moreover, various P3AT-based block copolymers can be prepared by exploiting the living characteristics of CTP reactions, facilitating studies of their unique properties and morphologies.[68,69] Another important approach for achieving high RR P3ATs is through cross-coupling polymerization reactions. Barker and co-workers obtained P3ATs with over 96% RR by Stille cross-coupling reactions with 2-iodo-5-Bu_3Sn-3-alkylthiophene (**K**).[70] Additionally, Bidan and co-workers adopted Suzuki coupling

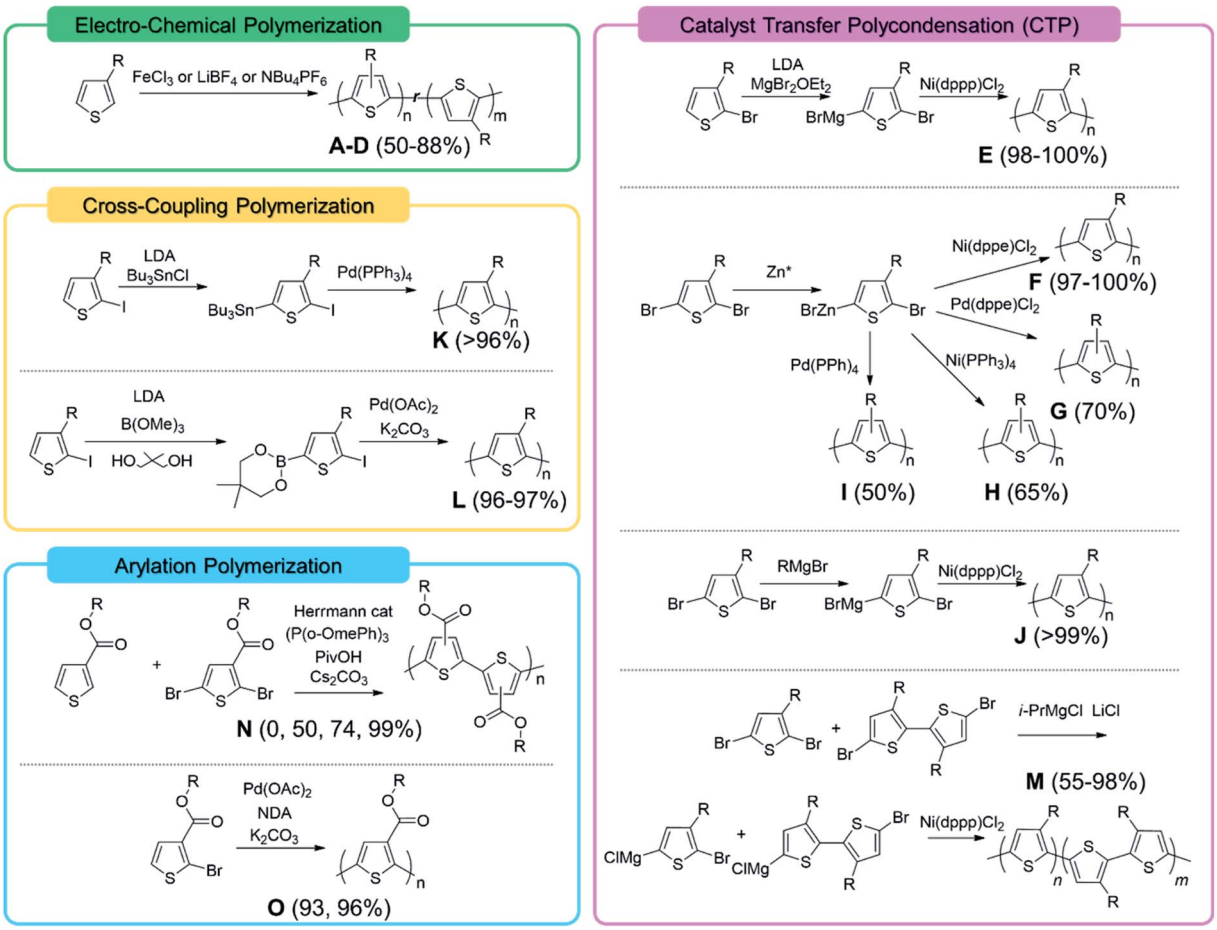

Fig. 2 Synthesis of P3ATs with different RRs *via* various methods: electro-chemical polymerization,[54–56] cross-coupling polymerization,[70,71] arylation polymerization,[75,76] and catalyst transfer polycondensation.[25,60–63,74]

Table 1 Various methods for the synthesis of P3ATs with different RRs

Label	Method	RR [%]	Reactant	Alkyl side chain	Catalyst	Solvent	Ref.
A	Chemical polymerization	50	3-Alkylthiophene	Butyl, hexyl, and icosanyl	$FeCl_3$	$CHCl_3$	54
B	Electro-polymerization	50	3-Alkylthiophene	Butyl, hexyl, and icosanyl	$LiBF_4$	MeCN	54
C	Electro-polymerization	70–80	3-Alkylthiophene	Hexyl, octyl, decyl, and dodecyl	NBu_4PF_6	$PhNO_2$	55
D	Chemical polymerization	68–88	3-Hexylthiophene	Hexyl	$FeCl_3$	$CHCl_3$	56
E	McCullough	98–100	2-Bromo-3-alkylthiophene	Butyl, hexyl, octyl, and dodecyl	LDA and $MgBr_2OEt_2$ $Ni(dppp)Cl_2$	THF	60
F	Rieke	97–100	2,5-Dibromo-3-alkylthiophene	Butyl, hexyl, octyl, decyl, dodecyl, and tetradecyl	ZnBr $Ni(dppe)Cl_2$	THF	61 and 62
G	Rieke	70	2,5-Dibromo-3-alkylthiophene	Hexyl	ZnBr $Pd(dppe)Cl_2$	THF	61
H	Rieke	65	2,5-Dibromo-3-alkylthiophene	Hexyl	ZnBr $Ni(PPh_3)_4$	THF	61
I	Rieke	50	2,5-Dibromo-3-alkylthiophene	Butyl, hexyl, and octyl	ZnBr $Pd(PPh_3)_4$	THF	61
J	GRIM	>99	2,5-Dibromo-3-alkylthiophene	Dodecyl	RMgX $Ni(dppp)Cl_2$	THF	63
K	Stille coupling	>96	2-Iodo-5-Bu_3Sn-3-alkylthiophene	Hexyl	$Pd(PPh_3)_4$	Tol	70
L	Suzuki coupling	96–97	2-Iodo-5-boronate-3-alkylthiophene	Octyl	$Pd(Oac)_2$, K_2CO_3	THF	71
M	GRIM	55–98	2,5-Dibromo-3-alkylthiophene 5′-Bromo-3,4′-dialkyl-5-bromo-[2,2′]-bithiophene	Hexyl and dodecyl	IsoPrMgCl $Ni(dppp)Cl_2$	THF	25 and 74
N	Arylation	0 and 50 74 and 99	3-Octyloxycarbonylthiophene 2,5-Dibromo-3-octyloxycarbonylthiophene	Octyl	Herrmann cat. (P(*o*-OmePh)$_3$) PivOH, Cs_2CO_3	Tol	75
O	Arylation	93 and 96	5-Dibromo-3-octyloxycarbonylthiophene	Hexyl	$Pd(OAc)_2$, K_2CO_3, and neodecanoic acid	DMA	76

condensation reactions to yield P3ATs with 96–97% RR (**L**).[71] Recently, ester-functionalized polythiophene with high regioselectivity could also be obtained through nickel-catalyzed Suzuki polycondensation.[72] Although air-free techniques are necessary for preparing organometallic monomers under cryogenic conditions, these palladium assisted cross-coupling methods produce well-defined P3ATs with RRs of over 96% (Table 1).

While several polymerization methods have been proposed for producing highly *rre* P3ATs, precise control of RR of P3ATs remains a great challenge. Fréchet *et al.* first suggested a simple synthetic method of controlling RR of poly(3-hexylthiophene) (P3HT) by copolymerizing the 3-hexylthiophene monomer and a H–H coupled 3,4′-dihexyl-2,2′-bithiophene dimer.[73] Later, Kim and co-workers further developed this method to extend the RR from 55 to 98% by controlling the monomer to H–H coupled dimer feed ratio (**M**).[25,74] Because this approach using the H–H coupled dimer is based on living GRIM polymerization, well-controlled molecular weight depending on the monomer/catalyst ratio and low-dispersity P3HT with precisely tuned RR could be achieved. Alternatively, RR of poly(3-octyloxycarbonylthiophene)s (P3OETs) can be controlled through palladium-catalyzed direct arylated polycondensation (DArP).[75,76] The DArP method is based on direct hetero C–H/C–H coupling, which does not require additional functionalization and metalation of the monomers for the polymerization. Gobalasingham *et al.* synthesized a *rre* P3OET with a RR higher than 93% using DArP polycondensation (**O**).[76] Later, Menda *et al.* reported a series of P3OETs with different RRs of 0, 50, 74, and 99%, which has been obtained depending on the combination of 3-octyloxycarbonylthiophene and 2,5-dibromo-3-octyloxycarbonylthiophene monomers (N).[75]

It is well known that the intrinsic properties of P3ATs are significantly impacted by the RR of their conjugated backbone. The presence of regio-defects (T–T and H–H bonds) in P3ATs induces a large steric hindrance between their alkyl substituents (Fig. 3). Thus, *rir* linkages in low RR P3ATs induce a steric twisting of the thiophene rings, resulting in short persistence lengths,[77] small effective conjugation lengths,[78] small crystallite thicknesses,[27] and more coil-like chain conformations.[79] Consequently, the properties of *rre* and *rra* P3ATs become completely different such as thermal properties, crystallinities, self-assembled morphologies, optoelectrical properties, and mechanical properties.

The RR of P3ATs is well-recognized as a key parameter for determining their crystalline properties (Fig. 4a). For example, the differential scanning calorimetry (DSC) profile of *rre* P3HTs shows a distinct endothermic peak and high T_m (~220 °C) from the melting of well-ordered crystallites, whereas no melting peak was observed for *rra* P3HTs, indicating their amorphous nature.[78,80] In particular, Kim *et al.* produced a series of P3HTs with a wide range of RR from 60 to 98% and compared their crystallization behaviors as a function of RR.[25] As the RR of the P3HTs decreased, T_m and ΔH_m gradually decreased, attributed to smaller crystalline domains with larger regio-defects. The degree of crystallinity of the P3HTs gradually decreased from 48 (RR = 98%) to 22% (RR = 80%) and to 16% (RR = 75%). When the RR of P3HT was lower than 75%, the crystallization of P3HT was significantly suppressed and no endothermic peaks from melting crystallites were observed by DSC. In addition to the bulk crystallization properties, RR-dependent crystal orientations in thin-films were investigated by Leeuw *et al.*[81] The crystal orientations in thin films, such as in the in-plane or out-of-plane direction, are particularly important for various organic electronic applications, *i.e.*, horizontal charge transportation in OFETs and vertical direction charge transport in PSCs. The *rre* P3ATs predominantly crystallize into edge-on oriented structures, showing sharp, high-order (*h*00) lamellar stacking in the out-of-plane direction, along with strong (010) in-plane π–π stacking. In contrast, the *rir* P3ATs adopt face-on oriented crystal structures, supported by weak (*h*00) peaks in the in-plane direction and distinct amorphous halo rings.[81–83]

Such RR dependent structural differences in the P3AT chains can significantly affect their self-assembly behavior. For example, strong π–π interactions in high RR P3HTs drive their unique one-dimensional assembly into nanowires (NWs), which act as highly effective long charge transport pathways in organic electronics (Fig. 4b).[84,85] In contrast, the average length of the NWs became much shorter as the RR decreased, and the *rra* P3HTs adopted irregular structures.[86] Thus, systematic RR modulation allows for precise control of the intermolecular interactions between CPs. For example, most P3HT-based block

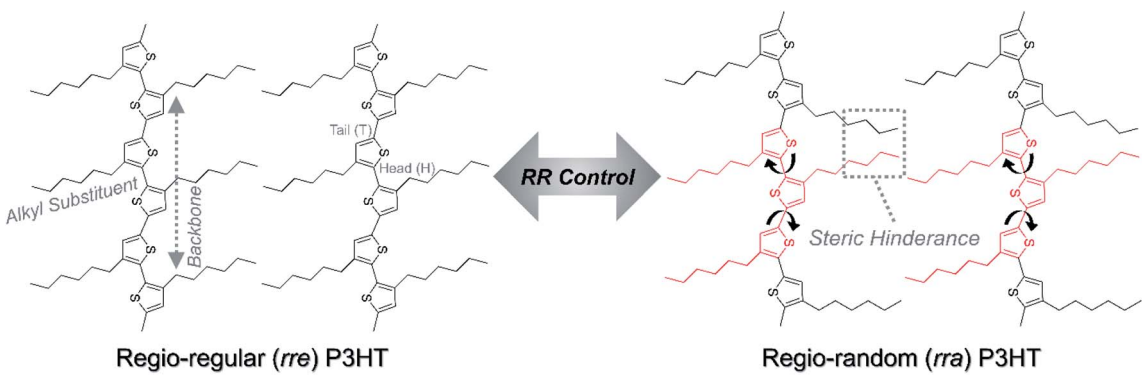

Fig. 3 Molecular structures of *rre* and *rra* P3HTs.

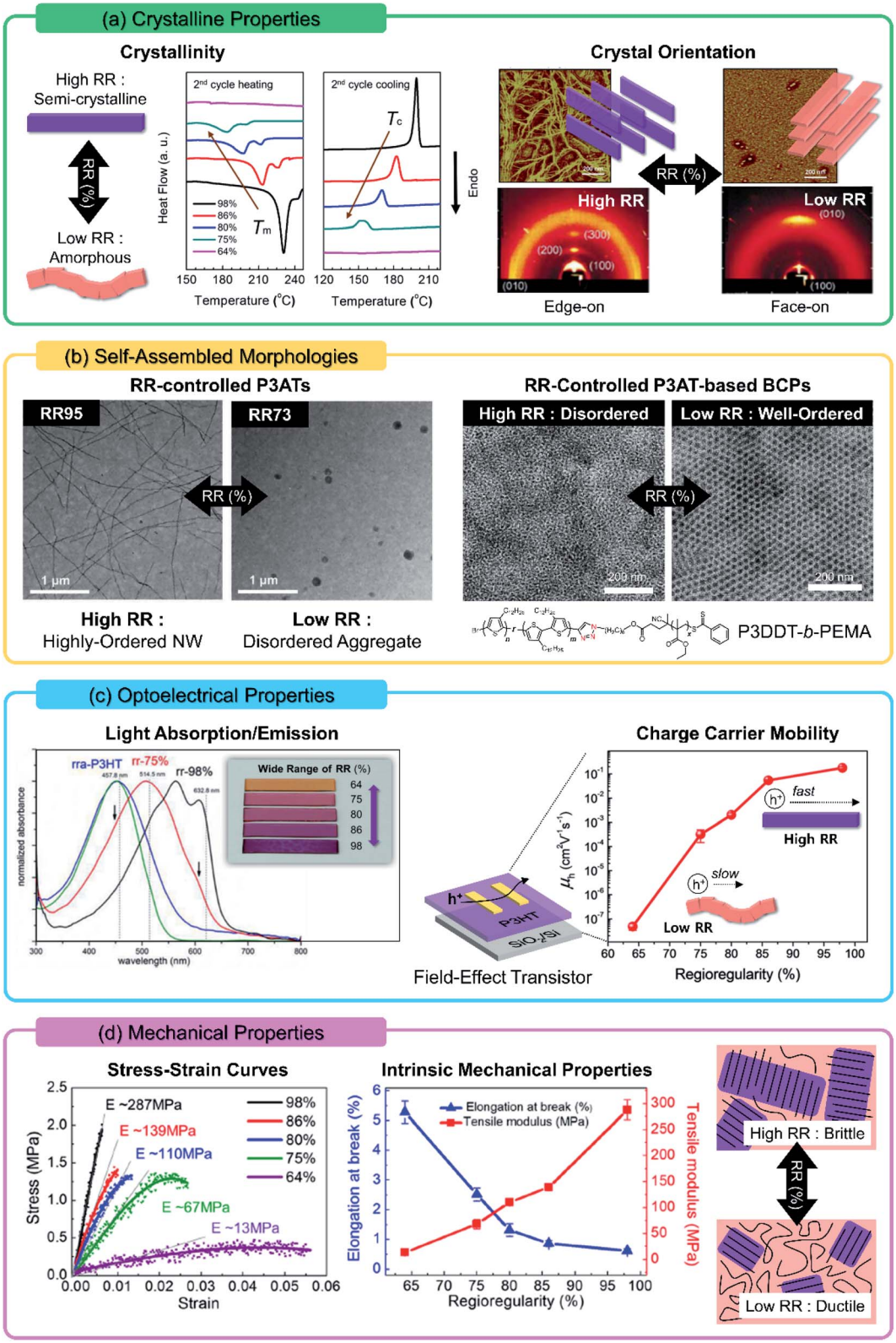

Fig. 4 Influences of RR on the (a) crystallinity, (b) self-assembled morphologies, (c) optoelectrical properties, and (d) mechanical properties of P3ATs as a function of RR. Reproduced with permission.[25,81,86,87,92] Copyright 2015, American Chemical Society, copyright 1999, Nature, copyright 2021, Elsevier, copyright 2019, Elsevier, and copyright 2018, American Chemical Society.

copolymers exhibit only fibril-like morphologies, irrespective of the type and volume fraction of the second block. This is because the strong crystallization in the P3HT block dominates the phase behaviors, resulting in kinetically trapped morphologies. Lowering the RR allows the formation of ordered nanostructures by weakening the initially strong molecular interactions in the P3HT blocks and, thus, enthalpic interaction can govern the phase behaviors of the block copolymers.[87–89]

These different self-assembled structures formed by *rre* and *rra* P3ATs result in significant differences in their optoelectrical properties (Fig. 4c). For example, the correlations between the RR-dependent chain conformations and the UV-vis absorption spectra of P3HTs were relatively well investigated.[90–92] High RR P3HTs showed distinct absorption peaks at around 2.09, 2.27, and 2.37 eV (600, 546, and 523 nm), corresponding to the vibronic coupling of π–π* transition. The ratio between the 0–0 peak (at 600 nm) and 0–1 peak (at 546 nm) was highly correlated with strong intra/interchain interactions in well-ordered crystallites (rod-like chain conformations).[93] In contrast, the absorption spectrum of the low RR P3HT was blue-shifted with a maximum peak and broad shoulder appearing at 2.72 eV (456 nm) and 3.0 eV (413 nm), respectively. These changes are attributed to a decrease in the effective conjugation length of amorphous P3HTs (coil-like chain conformations), which require more energy for electron excitation. Moreover, based on photoluminescence (PL) analysis, it was reported that the emissions of *rre* and *rra* P3HTs differed.[94,95] The emission spectrum of *rra* P3HTs showed a relatively weak and blue-shifted emission compared to that of *rre* P3HTs due to the weak intra/interchain interactions, similar to the trends observed for the UV-vis absorption spectra. Interestingly, photoexcitation dynamics of the *rre* P3HTs were completely different from those of the *rra* isomers, with a long fluorescence decay lifetime (576 ps), where the emission arising from only a single species (the first excited singlet exciton) participates as supported by the wavelength-independent quasi single exponential spectrum.[93,96] Thus, the suppressed interchain interactions in *rra* P3HTs promote faster energy transfer relaxation to generate low energy states.

The relationships between the RRs and electrical properties of P3ATs have been extensively examined by comparing the charge-carrier mobilities (μ) in OFETs (Fig. 4c). In the 1990s, it was first reported that *rre* P3ATs can afford a much higher value of μ (at least 2 orders of magnitude) compared to *rra* P3ATs.[97–99] As the RR decreases, the regio-defects in the polymer chains twist the polymer backbone, distorting the efficient charge transport pathway, thereby yielding a low μ. For instance, Leeuw *et al.* reported three orders of the magnitude improved μ from 2×10^{-4} to 1×10^{-1} $cm^2 V^{-1} s^{-1}$, by increasing the RR value from 81 to 96%, respectively.[81] In this regard, many researchers have made efforts to enhance μ by achieving very high RR of P3ATs.[100–104] High RR P3HTs form well-ordered intermolecular structures with broader delocalization of the π-electrons, leading to efficient charge transport pathways.

Lastly, the RR also influences the mechanical properties of P3ATs (Fig. 4d). Tuning the mechanical properties of CPs has recently emerged as an important parameter in the design of CPs, particularly for applications in wearable/portable electronics. Kim *et al.* compared the stretchability (crack-onset strain, COS) and tensile modulus of a series of P3HTs with various RR values (from 64 to 98%).[25] In the free-standing tensile test of P3HT thin films on water, a significant increase in the COS from 0.6 to 5.3% and a decrease in the tensile modulus from 287 to 13 MPa were observed for lower RR materials. The enhanced tensile strength and stretchability of low RR P3HTs are attributed to their large amorphous domains, allowing efficient stress relaxations by alignment of the chains in the strain directions. In contrast, excessive crystalline regions in high RR domains can act as an initial crack point, leading to low energy dissipations under strains, resulting in a mechanical failure even under low strain. When incorporated into flexible devices, P3HTs with a RR of 64% exhibited well-maintained current–voltage curves after 800 bending test cycles, whereas the 98% RR P3HTs failed after only 50 bending cycles. Thus, tuning the RR of CPs is an effective means of engineering the mechanical properties of CPs for various organic electronic applications. While there is typically a trade-off relationship between the mechanical and electrical properties of CPs depending on their RR values,[105] it is highly desirable to achieve both for efficient electronic devices including the flexible and stretchable devices.[15,106–113] In this regard, various strategies for developing robust, high performing conjugated materials have been reported. For example, blending the two polymers with different RRs or combining high RR and low RR blocks in one polymer chain can simultaneously optimize the mechanical and electrical performances (Fig. 5).[114–116]

2.3 RR of D–A copolymers

Most high-performance state-of-the-art CPs feature a D–A molecular configuration, where the D and A moieties are alternatively coupled along the conjugated backbones. D–A alternating polymers can afford advantageous optoelectronic properties through facile tuning of their optical bandgap, energy levels, and charge transport properties *via* intramolecular charge transfer (ICT) and orbital hybridization between D and A moieties. To exploit these features, numerous D–A CPs have been developed to date with remarkable improvements in their optoelectronic performance. Despite extensive studies on the molecular designs for D–A CPs, the effect of RR on D–A copolymers has been largely unexplored. In particular, the RR is now emerging as a particularly important parameter for high-performance D–A CPs since their chemical structures become more complex with larger molecular asymmetry. We examine the impact of RR on various D–A copolymers by reviewing a library of recently developed D–A type CPs with controlled RR. The CPs are classified into three types depending on the RR (directional, positional, and sequential RRs).

2.3.1 Directional RR of D–A copolymers. The directional RR of D–A type CPs can be defined by the directional orientation of the functional groups or side chains along the conjugated backbones, as similar to the RR of P3ATs.[30–34] An excellent example of controlling the directional RR of D–A copolymers

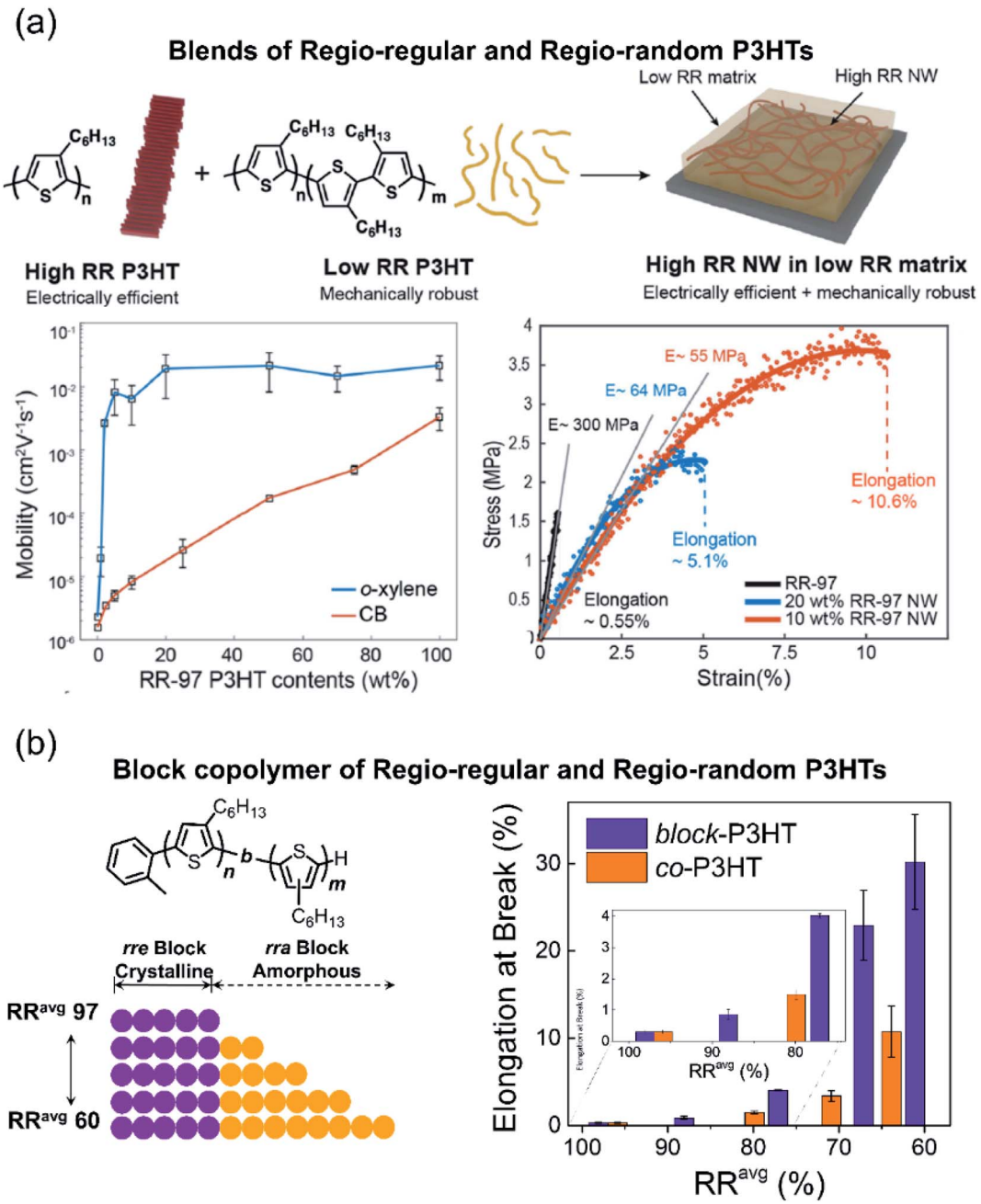

Fig. 5 Flexible and stretchable electronics with the incorporation of *rre* P3HTs into *rra* P3HTs using the (a) blend and (b) block copolymer approach, respectively. Reproduced with permission.[114,115] Copyright 2017, American Chemical Society, and copyright 2019, American Chemical Society.

was demonstrated with the PTB7-Th D–A copolymer, which is one of the most successful donor materials used in high-performance PSCs. In general, PTB7-Th is prepared by the poly-condensation reaction of the electron-rich [2,6′-4,8-di(5-ethylhexylthienyl)benzo[1,2-*b*:3,3-*b*]dithiophene] (BDTT) moiety with the electron-deficient fluoro-substituted thieno[3,4-*b*]thiophene (FTT) moiety.[36] However, the FTT unit in PTB7-Th contains asymmetric reactive sites at the 4- and 6-positions, resulting in two distinct regio-isomers. In order to produce *rre* PTB7-Th, the FTT-BDTT-FTT trimer (M2) was first prepared (Fig. 6a). Polymerization of the dibromo-M2 trimer with ditrimethyltin-BDTT by Stille coupling reactions yielded *rre* PTB7-Th (P2). On the other hand, *rra* PTB7-Th (P3) was synthesized by polymerizing ditrimethyltin-BDTT and dibromo-FTT through Stille coupling condensation reactions. Thereafter, Bo *et al.* also demonstrated a similar method of preparing directionally *rre* and *rra* poly[(2,6-(4,8-bis(5-(2-ethylhexyl)thiophene-2-yl)-benzo[1,2-*b*:4,5-*b*′]dithiophene))-*alt*-(2,5-(ethyl thiophene carboxylate))] (PThE) D–A copolymers by the polymerization of symmetric D–A–D trimers and an A monomer (Fig. 6b).

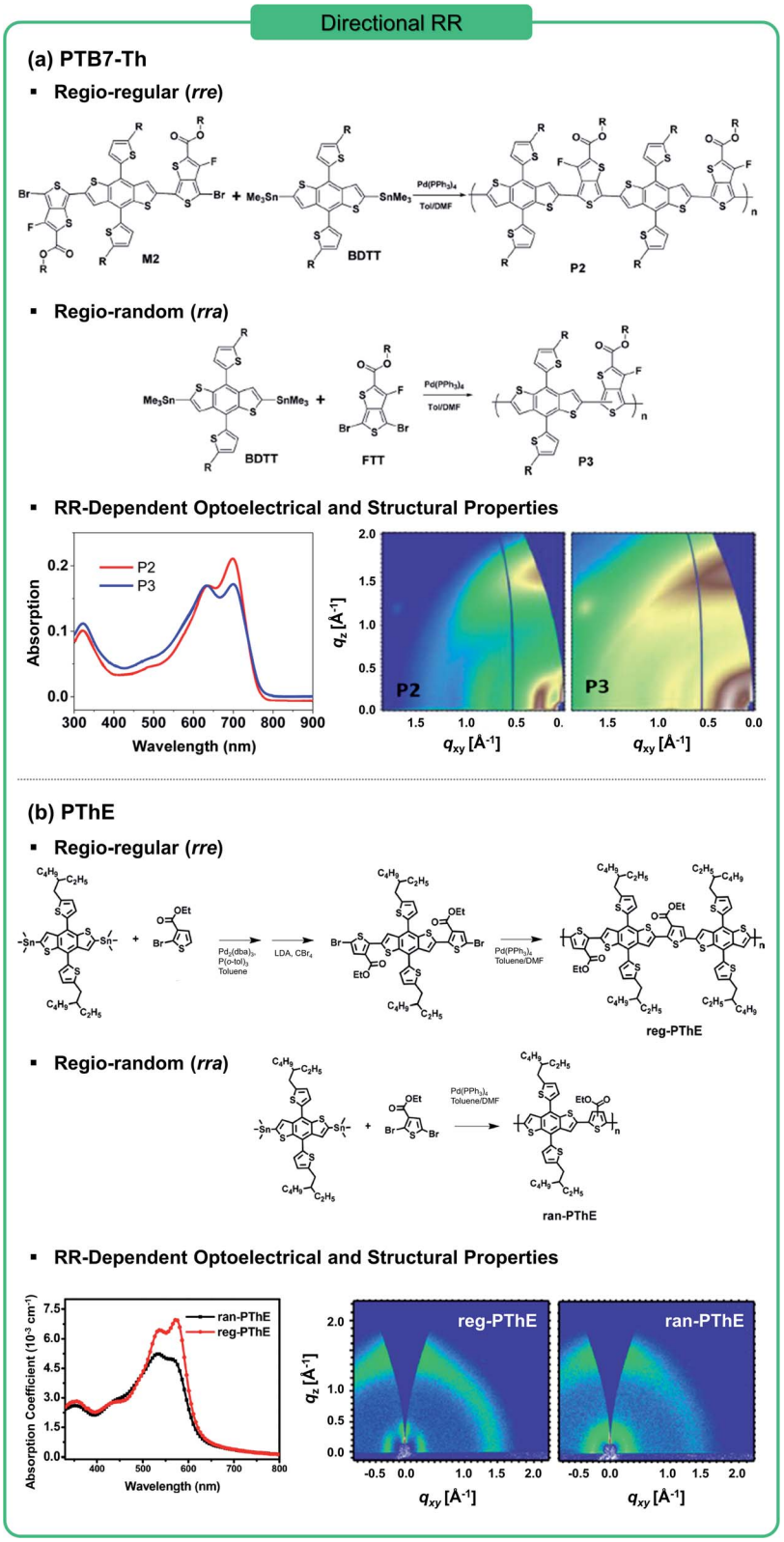

Fig. 6 Influences of RR on the opto-electrical and structural properties of D–A copolymers with directional RR: (a) PTB7-Th; and (b) PThE. Reproduced with permission.[30,36] Copyright 2018, American Chemical Society, and copyright 2017, Royal Society of Chemistry.

Comparative analysis of directionally *rre* and *rra* D–A copolymers demonstrated that the directional RR of the side chains or functional groups exerts an influence on their light absorption, packing order, and charge mobility. These structure–property relationships result from cooperative molecular arrangements of the functional side groups. These

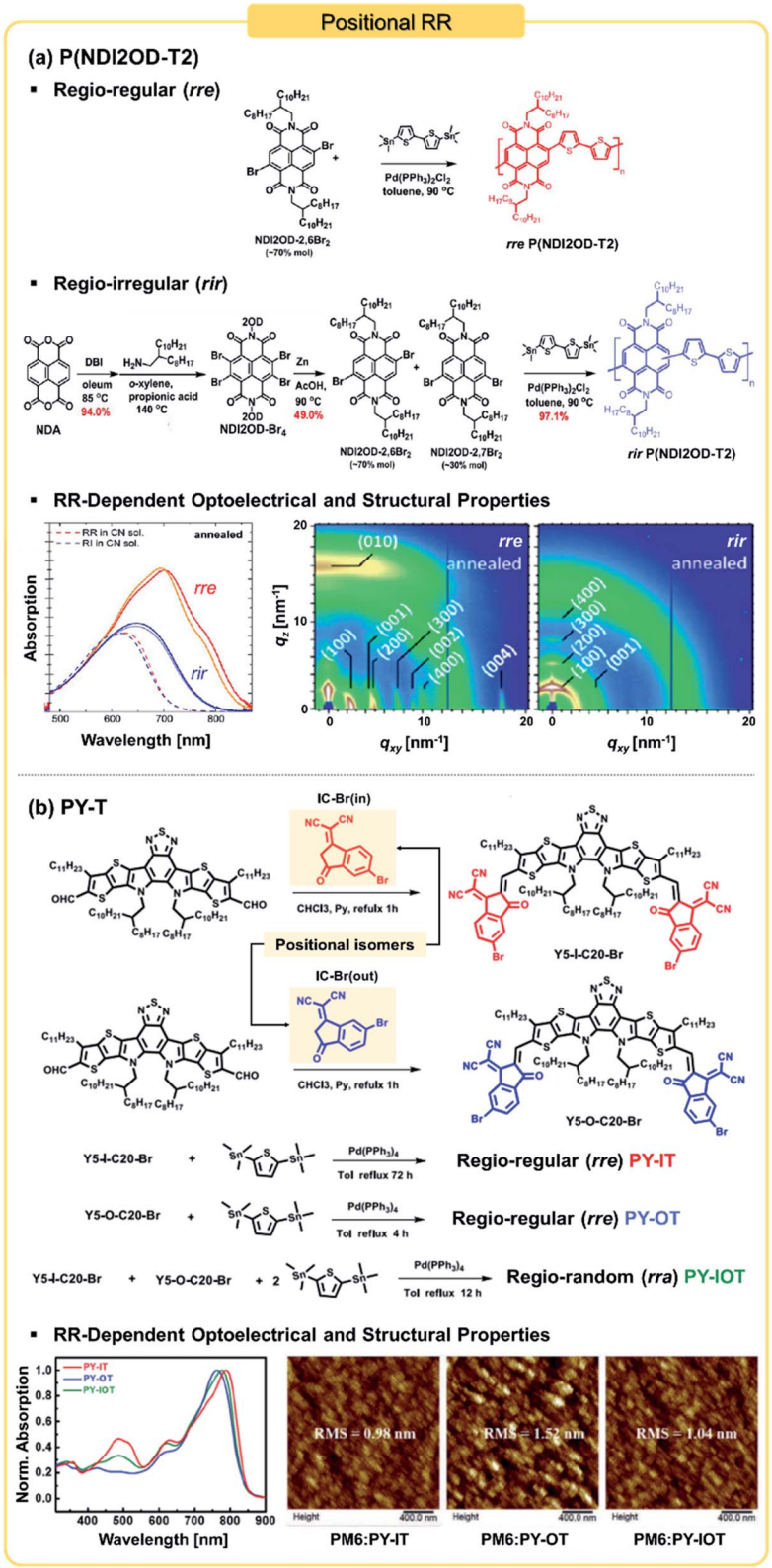

Fig. 7 Influences of RR on the structural and optoelectrical properties of D–A copolymers with positional RR: (a) P(NDI2OD-T2); and (b) PY-T. Reproduced with permission.[41,43] Copyright 2021, American Chemical Society, and copyright 2014, American Chemical Society.

arrangements affect the noncovalent interactions with aromatic protons on the conjugated backbone and the planarity of the CP chains. For example, the absorption coefficients of *rre* PThE and *rra* PThE in thin films were estimated to be 6.98×10^3 cm^{-1} and 5.23×10^3 cm^{-1}, respectively.[30] Although these two polymers exhibit similar absorption ranges, their relative intensities of the peaks were different. *rra* PThE showed a stronger absorption peak at 532 nm and a weaker absorption peak at 573 nm, meanwhile *rre* PThE showed the opposite trend, indicating that *rre* PThE has stronger inter-chain interactions than *rra* PThE in

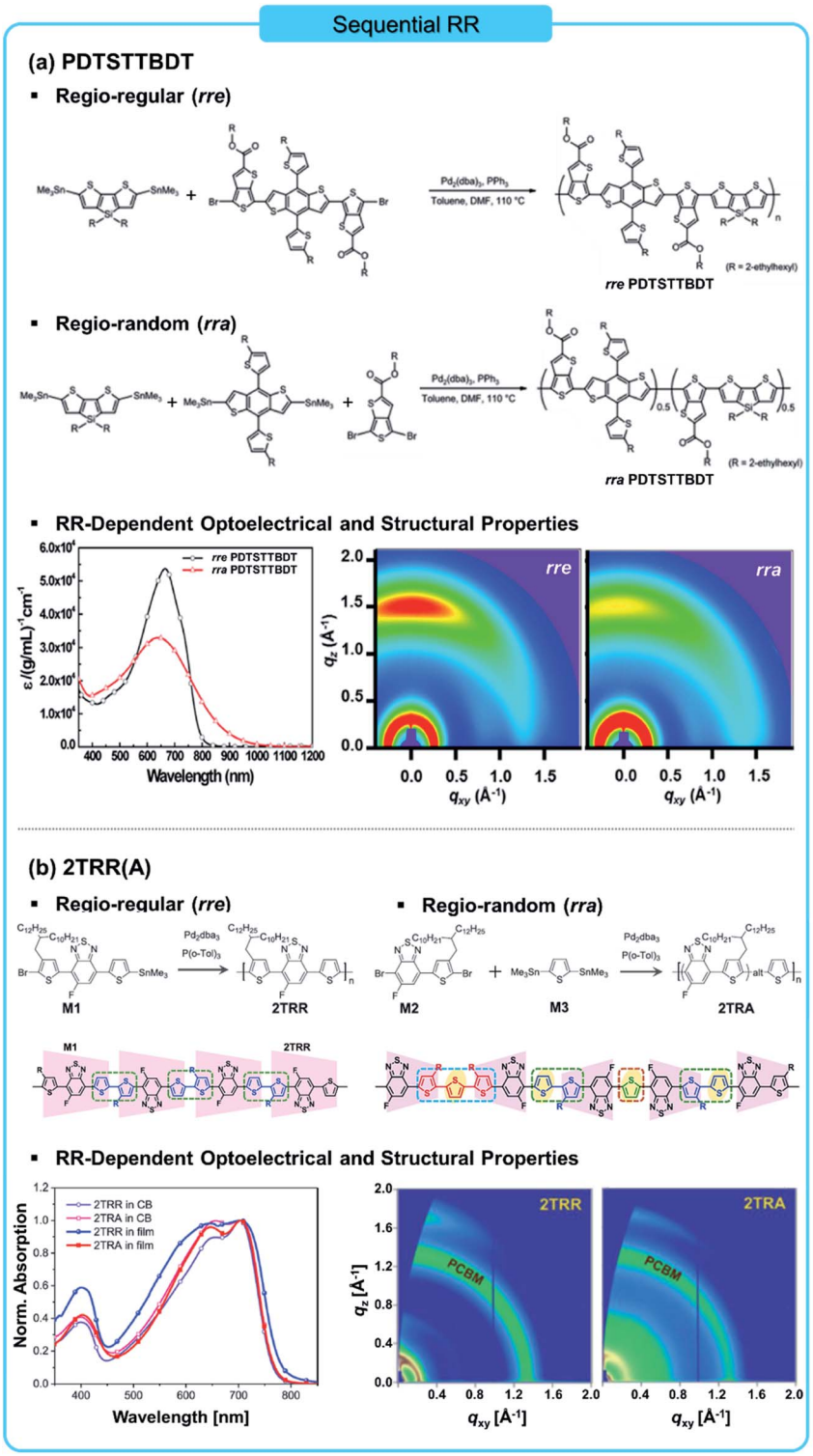

Fig. 8 Influence of RR on the structural and optoelectrical properties of D–A copolymers with sequential RR: (a) PDTSTTBDT; and (b) 2TRR(A). Reproduced with permission.[46,48] Copyright 2016, American Chemical Society, and copyright 2017, Wiley.

thin films. The grazing incidence X-ray scattering (GIXS) pattern shows that the peaks of the lamellar structures in *rre* PThE disappeared in *rra* PThE, suggesting that the high RR induced higher crystallinity and stronger intermolecular interactions, consistent with the UV-vis spectra. Differences in the optoelectrical features of directionally *rre* and *rra* D–A copolymers have also been reported in other D–A copolymer systems.[31–34] Note that directional RR dependent optoelectrical properties in D–A copolymers are less significant than the changes observed in P3ATs. Considering the small fraction of functional groups, related to directional RR in D–A copolymers compared to the whole molecule, the steric effect from RR defects within D–A copolymers is not as significant as in the case of homopolymers with asymmetric alkyl chains. Moreover, the limited M_n and high dispersity of the *rre* D–A copolymers originating from the step-growth polymerization methods may result in less ordered structures.

2.3.2 Positional RR of D–A copolymers. A successful example of positional RR in D–A copolymers was demonstrated by Neher and co-workers using the regio-isomers of P(NDI2OD-T2).[43] In the acceptor moiety (NDI2OD) of P(NDI2OD-T2), four different hydrogen positions can be substituted as reactive sites for the polymerization, resulting in either 2,6- or 2,7-conformations between the D and A monomer units. The key for obtaining *rre* P(NDI2OD-T2) is the use of *N*,*N*′-bis (2-octyldodecyl)-2,6-dibromonaphthalene-1,4,5,8-bis-(dicaroximide) (NDI2OD-2,6-Br_2) as a building block (Fig. 7a). Polymerization at the 2,6-bromide on the NDI backbone leads to the formation of a regio-selective polymer in which the monomers are diagonally oriented along the chain. Meanwhile, positionally *rir* P(NDI2OD-T2) can be produced by using a mixture of NDI2OD-2,6-Br_2 and NDI2OD-2,7-Br_2. In the synthesis of *rir* P(NDI2OD-T2), NDI2OD-Br_4 was first prepared by tetrabromination of 1,4,5,8-naphthalenetetracarboxylic dianhydride (NDA) with dibromoisocyanuric acid, which was subsequently reacted with 2-octadecylamine. Then, the tetrabromoimide system was randomly debrominated using Zn catalysts to obtain a mixture of brominated NDI (70% of NDI2OD-2,6Br_2 and 30% of NDI2OD-2,7Br_2). Finally, the dibromide isomer mixture was reacted with 5,5′-bis(trimethylstannyl)-2,2′-dithiophene using the $Pd(PPh_3)_2Cl_2$ catalyst to obtain a positional *rir* copolymer.

Another good example of the positional RR in D–A copolymers is polymerized small-molecule-acceptors (PSMAs),

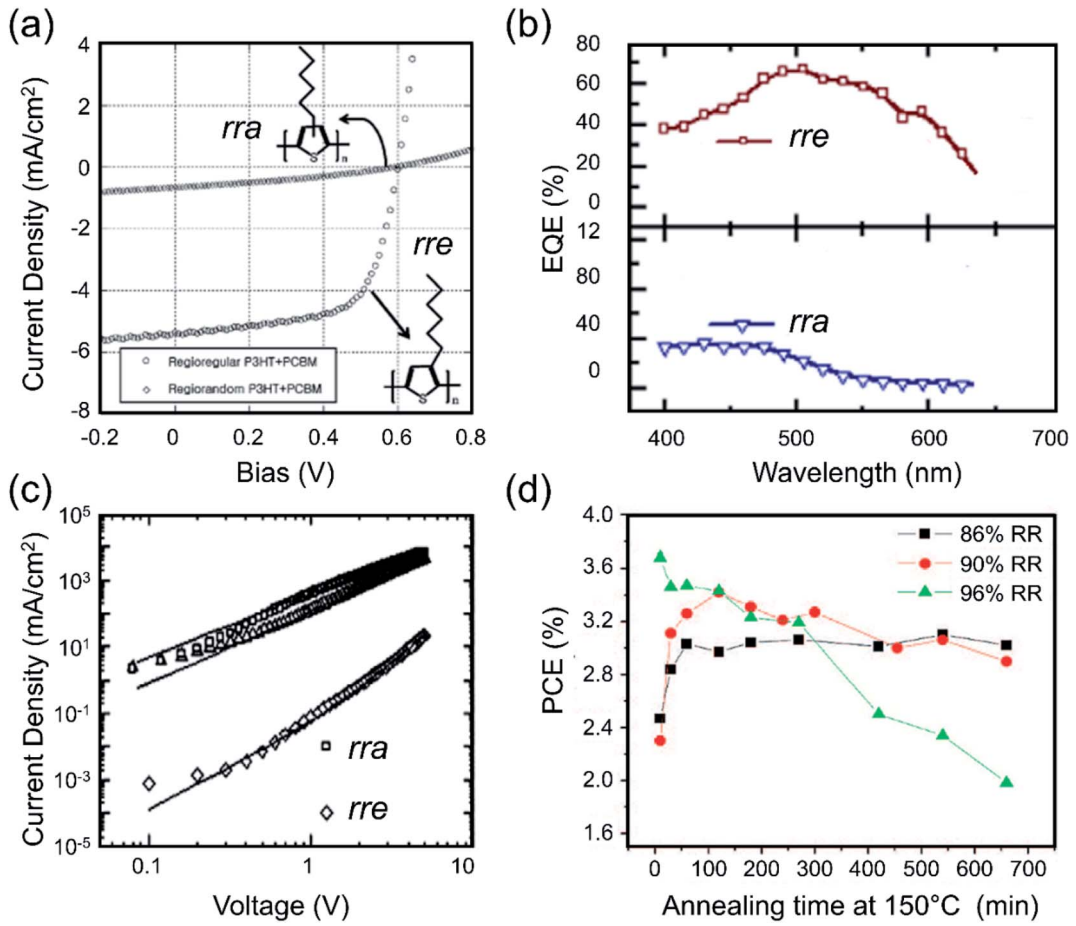

Fig. 9 (a) Current density–voltage curves, (b) EQE curves, and (c) SCLC curves of BHJ-PSCs using blends of *rre*- and *rra* P3HT:PCBM. (d) Thermal stability of P3HT:PCBM PSCs with different RRs. Reproduced with permission.[83,184,185] Copyright 2008, American Chemical Society, copyright 2009, Elsevier, and copyright 2009, American Chemical Society.

a recently developed class of high-performance polymer acceptors. In these systems, non-fullerene small-molecule-acceptor (NFSMA) with multiple fused rings and strong dyes are alternatively copolymerized with donating spacers (*i.e.*, thiophene or selenophene) to yield polymerized NFSMAs (PSMAs).[39–41,117,118] The reactive bromides on different positions on the SMA monomer (*i.e.*, 1,1-dicyanomethylene-3-indanone (IC-Br)) result in two different positional isomers of IC-Br units (IC-Br(in) and IC-Br(out)) based on their position relative to other functional groups (*i.e.*, carbonyl and malononitrile groups) (Fig. 7b).[39] Thus, the polymerization of these IC-Br SMA monomers results in three different positional-isomeric pairs (*i.e.*, in/in, in/out, and out/out). Therefore, most early-stage PSMAs have *rra* arrangements along their polymer backbones. RR-controlled PSMAs were recently developed by separating out isomerically pure IC-Br units through recrystallization in different solvents (*i.e.*, $CHCl_3$ for IC-Br(in) and ethanol for IC-Br(out)). For example, Luo and co-workers developed two different RR-controlled PSMAs (PY-IT and PY-OT) using separated IC-Br(in) and IC-Br(out) for each polymer, and compared them with the *rra* PSMA (PY-IOT) containing a mixture of IC-Br units (Fig. 7b). Also, Jen and co-workers synthesized RR-controlled benzotriazole-based PSMAs (*rre* PZT-γ) by using separated IC-Br(in) during polymerization, and compared it with the *rra* PZT counterparts.[41]

Positional RR significantly impacts the backbone conformation of CPs by inducing tilts between the D and A units. To study these effects, Neher *et al.* compared the optical and structural properties of P(NDI2OD-T2) with different positional RR.[43] The absorption range of positionally *rre* P(NDI2OD-T2) shifted toward a lower wavelength compared to that of the *rir* derivatives, as shown in Fig. 7a. Notably, *rre* P(NDI2OD-T2) produced two different aggregate species in thin-films. The intrachain aggregation was shown in the absorption peak at ~700 nm and the interchain aggregation was found in the shoulder peak at ~790 nm. Meanwhile, such vibronic peaks were not found in the spectrum of *rir* P(NDI2OD-T2), indicating that positional RR affects the intermolecular assembly of CPs. This was also supported by the GIXS plots. Two distinct crystal packing structures were observed corresponding to *rre* and *rir* P(NDI2OD-T2). Bar-shaped scattering peaks were observed in the spectrum of the *rre* polymer film, suggesting a long-range ordering of the crystallites. Later, RR-controlled P(NDI2OD-T2) s were demonstrated by Ludwigs and co-workers by polymerizing 2,6- and 2,7-NDI regio-isomers having various feed ratios.[42] Through this system, a gradual hypochromic shift as well as decreased crystal ordering and electron mobility were observed as the positional RR decreased. In contrast to P3ATs where low RR leads to an amorphous film, *rir* P(NDI2OD-T2) exhibits rather unique two-dimensional ordered microstructures as it is less aggregated in the solution state. This unique feature of positional RR-controlled P(NDI2OD-T2) allows for charge transport along different crystallographic axes. In addition, the different RRs of PSMAs drove clear transitions in their optical and morphological properties. For example, *rre* PY-IT had a red-shifted absorption region compared to the *rra* PY-IOT, while the other form of *rre* PSMA (PY-OT) had blue-shifted absorption compared with the *rra* one (PY-IOT) (Fig. 7b). Also, surfaces of blend films with a polymer donor (PM6) linearly got rougher in the order of PY-IT, PY-IOT, and PY-OT, suggesting the importance of selectively controlling positional isomers when designing PSMAs.

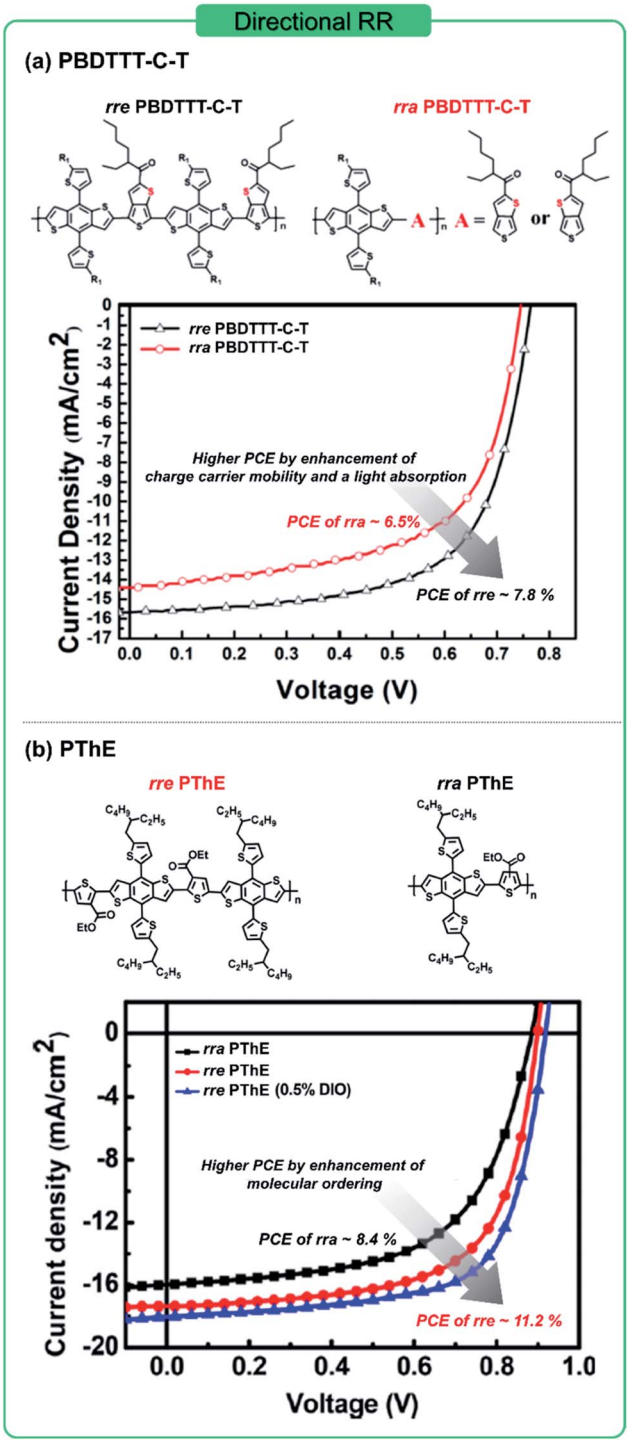

Fig. 10 Influences of RR on PCEs of PSCs based on D–A copolymers with directional RR: (a) PBDTTT-C-T; and (b) PThE. Reproduced with permission.[30,35] Copyright 2018, American Chemical Society, and copyright 2015, American Chemical Society.

2.3.3 Sequential RR of D–A copolymers. Sequential RR in D–A copolymers can be defined by the fraction of identical D–A sequences in the CPs. If the D and A monomers have asymmetric molecular structures, then the H–H or H–T arrangement between D–A will induce the formation of sequential regioisomers along the polymer backbone. Moreover, different repeating sequences can be obtained in D–A terpolymers (D–A1–D–A2) or tetrapolymers (D1–A1–D2–A2). There are several synthetic routes to control sequential RR. The first representative example is the synthesis of PDTSTTBDT consisting of dithieno[3,2-*b*:2′,3′-*d*]silole (DTS), benzo[1,2-*b*:4,5-*b*]dithiophene (BDT), and thieno[3,4-*b*]thiophene (TT) (Fig. 8a). *rre* PDTSTTBDT was synthesized by polymerizing a symmetric TT–BDT–TT trimer and a DTS monomer *via* Stille cross-coupling reactions. Sequentially *rra* PDTSTTBDT was synthesized from a mixture of TT (2 eq.), BDT (1 eq.), and DTS (1 eq.) where BDT and DTS equally compete to react with TT. As a second example, sequential RR in Ph–DPP–Ph–BDT was controlled by using a trimer.[46] The *rre* Ph–DPP–Ph–BDT terpolymer was synthesized from a symmetric trimer (Ph–DPP–Ph) and BDT. In contrast, a *rra* terpolymer was obtained by polymerizing an asymmetric trimer (Ph–DPP–Th or Ph–DPP–TT) and BDT. In addition, sequentially *rre* D–A copolymers have been demonstrated by the self-condensation of D1–D2–A trimers, which were selectively functionalized with two different reactive groups (*e.g.* Br and $SnMe_3$). One example is the copolymer of 5-fluorobenzothiadiazole (FBT), 3-(2-octyldodecyl)-thiophene (3ODT), and thiophene (T), reported by Cao and co-workers (Fig. 8b).[48] To synthesize the *rre* polymer (2TRR), the 3ODT-FBT-T trimer was self-polymerized, ensuring an identical $(D–A)_n$ sequence within the polymer backbone where D is the 3ODT–T dimer and A is the FBT monomer. On the other hand, the *rra* polymer (2TRA) was synthesized from a FBT–3ODT dimer and a T monomer. The random copolymerization of 3ODT and T afforded three donors that contain mono, di, or trithiophene in a single polymer chain. Thus, regio-selective self-condensation of D–A units or incorporating symmetric trimers is key for obtaining sequentially controlled conjugated materials.

Compared to directional and positional RR, sequential RR typically has more significant impacts on the optoelectrical properties as the conjugations between repeating units are directly varied. In the UV-vis absorption spectra, both the absorption coefficient and wavelength are widely tuned depending on the sequential RR of the CPs.[45–49] For example, *rre* PDTSTTBDT exhibited stronger ICT transitions than the *rra* counterpart, resulting in a blue shift of its absorption wavelength.[46] The frontier orbitals of the *rre* segments extend across the entire polymer backbone, contributing to a sharp onset and narrow band of electron transition. The absorption spectra of the *rra* polymers are broadened due to the different sequences in the random conjugated backbone. The broadening of the absorption spectra at lower and higher wavelengths can be assigned to continuous –BDT– fragments and –DTS– fragments, respectively. Thus, the light-absorption profile of random terpolymers with various chemical compositions can be tuned over a broad wavelength range.[119–125] Notably, the absorption coefficient of *rre* PDTSTTBDT is significantly higher than that of *rra* polymer, indicating the highly efficient light harvesting capabilities. In addition to its optoelectrical properties, *rre* PDTSTTBDT exhibited higher order peaks in the GIXS pattern compared to that of the *rra* analog, suggesting that the molecular ordering of the D–A copolymers can be enhanced when the sequential RR is controlled.[46]

3. Effects of RR on polymer solar cells (PSCs)

Among the many types of organic electronic devices, PSCs have attracted great attention as next-generation energy devices owing to their advantages such as solution processability, light weight, color tunability and mechanical flexibility.[126–131] After the first-generation PSCs based on bulk

Table 2 PCEs of directional *rre*- and *rra*-copolymer based PSCs

RR type	Active layer	RR	PCE [%]	$\mu_{h,SCLC}$ [$cm^2\ V^{-1}\ s^{-1}$]	$\mu_{e,SCLC}$ [$cm^2\ V^{-1}\ s^{-1}$]	Ref.
Directional	***rre* PBDTTT-C-T**:$PC_{71}BM$	*rre*	7.79	1.16×10^{-3a}	—	35
	***rra* PBDTTT-C-T**:$PC_{71}BM$	*rra*	6.60	5.02×10^{-4a}	—	
	***rre* PThE**:ITTC	*rre*	10.14	5.24×10^{-5}	5.76×10^{-5}	30
	***rra* PThE**:ITTC	*rra*	8.38	1.12×10^{-5}	2.65×10^{-5}	
	P2:$PC_{71}BM$	*rre*	9.97	—	9.76×10^{-3}	36
	P3:$PC_{71}BM$	*rra*	7.88	—	7.27×10^{-3}	
	PBDT-TSR:$PC_{71}BM$	*rre*	10.20	3.16×10^{-2a}	—	31
	PBDT-TS1:$PC_{71}BM$	*rra*	9.74	$8.78 \times 10^{-3\ a}$	—	
	PIPCP:$PC_{61}BM$	*rre*	6.13	1.4×10^{-4a}	—	33
	PIPC-RA:$PC_{61}BM$	*rra*	1.67	1.3×10^{-5a}	—	
	***rre*-(D_1–A–D_2–A)**:P_A	*rre*	5.93	3.1×10^{-4a}	—	32
	***rra*-(D_1–A–D_2–A)**:P_A	*rra*	4.72	3.9×10^{-5a}	—	
	PBTzT-4R:$PC_{71}BM$	*rre*	9.63	4.25×10^{-4}	—	34
	PBTzT-4:$PC_{71}BM$	*rra*	9.36	2.08×10^{-4}	—	
	PBTzT-6R:$PC_{71}BM$	*rre*	9.12	2.44×10^{-4}	—	
	PBTzT-6:$PC_{71}BM$	*rra*	8.52	1.16×10^{-4}	—	

[a] The mobility was measured with pristine polymer films (not blend).

heterojunction (BHJ) blends of p-type CPs as a polymer donor (P_D) and n-type fullerene derivative as an electron acceptor were reported, the power conversion efficiency (PCE) of PSCs has been dramatically increased to 17–18%, driven by the development of a wide variety of CPs and NFSMAs.[132–137] In particular, the advent of high-performance D–A type CPs with

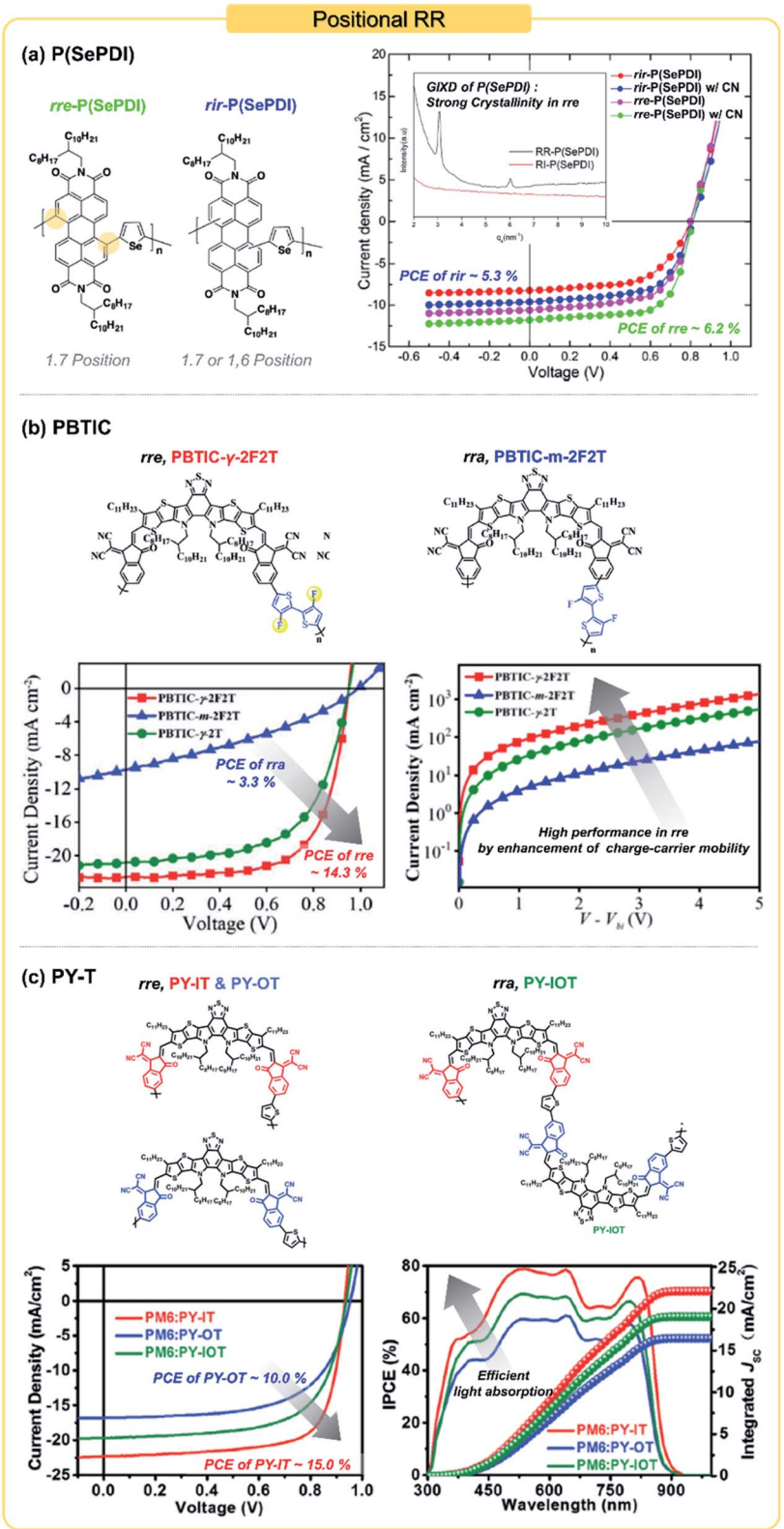

Fig. 11 Examples of PSCs employing D–A copolymers with different positional RRs: (a) P(SePDI); (b) PBTIC; and (c) PY-T. Reproduced with permission.[38,39,167] Copyright 2018, American Chemical Society, copyright 2020, Wiley, and copyright 2021, Wiley.

a capability of tunable energy levels and light absorption properties has led to remarkable improvements in the efficiency. By using these D–A copolymers as both P_Ds and polymer acceptors (P_As), efficient all-polymer solar cells (all-PSCs) have been achieved.[2,5,137–150] Engineering of the light absorption and frontier energy levels of both P_D and P_A affords simultaneous enhancements of the open-circuit voltage (V_{oc}) and short-circuit current density (J_{sc}), resulting in high-performance all-PSCs. Importantly, the P_D and P_A chains can be tie molecules and form entangled networks in the BHJ blends, thus resulting in superior mechanical/thermal stabilities and making all-PSCs as promising candidates for wearable and stretchable electronics.[151–157] Moreover, recent development of A–D–A (or A–D–A′–D–A) type NFSMAs including Y-series has afforded state-of-the-art PSCs with PCEs of over 18%.[158–165] However, NFSMA-based PSCs exhibit relatively poor mechanical and thermal stability. Thus, new D–A type polymer acceptors (PSMA) have been developed by polymerizing NFSMAs and other donating building blocks.[39–41,117,166–181] Because different regio-isomers are found in the chemical structures of NFSMA molecules, controlling the RR of the PSMA is an emerging factor for their design and application in high-efficiency all-PSCs. In this section, we will review a library of examples of RR control in the photovoltaic polymers and summarize the impacts of directional, positional, and sequential RRs on the PSC performance.

3.1 RR of homopolymers

In early studies on PSCs, P3ATs were the prototype p-type material for the active layers in PSCs.[182–185] In particular, P3HTs are often used as a model CP for BHJ PSCs for exploring general relationships between the primary structure and device function. Among several key variables, the RR of P3HTs has been identified as a primary factor for producing high-efficiency PSCs (Fig. 9). For example, Kim *et al.* demonstrated the strong influence of the RR on PSC performance, attributed to the enhanced optical absorption and charge transport in the well-ordered high RR P3HTs.[188] Consequently, optimal device efficiencies were achieved with the highest RR P3HTs. As shown in Fig. 9a, the current–voltage curves indicated that *rre* P3HTs produced much higher J_{sc} and fill factor (FF) than those of *rra* P3HTs due to its much lower series resistance (R_S, 3.6 Ω cm^2) compared to *rra* P3HTs (13 Ω cm^2). From the external quantum efficiency (EQE) curve, it was determined that *rre* P3HTs absorbed light over a wider range than *rra* P3HTs with higher photon-to-electrical conversion (Fig. 9b). The space-charge limited current (SCLC) measurements in Fig. 9b show that the hole mobility of *rre* P3HTs was almost 5 times higher than that of *rra* P3HTs. However, the excessive crystallization of high RR P3HTs can adversely affect the stability of the PSCs. The strong crystallization of the high RR P3HT greatly reduces its solubility and induces excessive phase separation with fullerene acceptors, decreasing the thermal and morphological stability of the PSCs.[179] For example, Fréchet and co-workers reported that increasing the RR and crystallinity resulted in more severe phase separation with PCBM under persistent heating.[83] As shown in Fig. 9d, P3HTs with 86% RR afforded a high PCE of over 3%, and enabled the fabrication of a thermally-stable PSC due to reduced phase separation with fullerene acceptors. In contrast, P3HTs with 96% RR exhibited the highest initial PCE, but the PCE declined significantly with exposure to thermal stress (at 150 °C). Thus, RR control is an important parameter for optimizing the blend morphology to achieve both high PCE and thermal stability of the P3HT-based PSCs.

Table 3 PCEs of positional *rre*-, *rir*-, and *rra*-copolymer based PSCs

RR type	Active layer	RR	PCE [%]	$\mu_{h,SCLC}$ [cm^2 V^{-1} s^{-1}]	$\mu_{e,SCLC}$ [cm^2 V^{-1} s^{-1}]	Ref.
Positional	P3HT:***rre*-PDI-diTh**	*rre*	2.17	—	5×10^{-4}[a]	37
	P3HT:***rir*-PDI-diTh**	*rir*	1.55	—	3×10^{-4}[a]	
	PTB7-Th:***rre*-P(SePDI)**	*rre*	6.2	3.59×10^{-4}	5.43×10^{-4}	38
	PTB7-Th:***rir*-P(SePDI)**	*rir*	5.3	7.25×10^{-5}	3.51×10^{-4}	
	PDCBT:**RR-P(NDI2OD-T2)**	*rre*	0.75	—	7×10^{-2}[a]	42
	PDCBT:**RI(70:30)**	*rir*	1.37	—	2×10^{-3}[a]	
	PDCBT:**RI(47:53)**	*rir*	2.42	—	3×10^{-3}[a]	
	PDCBT:**RI(24:76)**	*rir*	2.02	—	9×10^{-4} [a]	
	PM6:**L15**	*rre*	15.22	—	9.3×10^{-4}[a]	117
	PM6:**L14**	*rra*	14.41	—	8.7×10^{-4}[a]	
	PBDB-T:**PZT-γ**	*rre*	15.8	—	7.53×10^{-4}	41
	PBDB-T:**PZT**	*rra*	14.5	—	5.75×10^{-4}	
	PM6:**PY-IT**	*rre*	15.05	9.21×10^{-4}	5.28×10^{-4}	39
	PM6:**PY-OT**	*rre*	10.04	8.79×10^{-4}	3.81×10^{-4}	
	PM6:**PY-IOT**	*rra*	12.12	9.03×10^{-4}	4.57×10^{-4}	
	PM6:**PYF-T-o**	*rre*	15.2	8.4×10^{-4}	7.8×10^{-4}	40
	PM6:**PYF-T-m**	*rre*	1.4	1.2×10^{-4}	2.7×10^{-4}	
	PM6:**PYF-T**	*rra*	14.0	7.3×10^{-4}	6.5×10^{-4}	

[a] The mobility was measured with pristine polymer films (not blend).

3.2 RR of D–A copolymers

3.2.1 Directional RR of D–A copolymers. Similar to the cases of P3HT-based PSCs, the PCEs and stabilities of the PSCs based on D–A copolymers are largely affected by the directional RR. The *rre* polymers are more likely to aggregate and to have higher crystallinity than *rra* counterparts, attributed to the consistent arrangement of side chains or functional groups in the *rre* polymers. These features afford enhanced charge mobility and less charge recombination in the BHJ, and thus higher PCEs can be obtained from *rre* polymers (Fig. 10 and Table 2). For example, Lee and co-workers developed two different P_D (directionally *rre* and *rra* PBDTTT-C-T) and employed them in PSCs with the $PC_{71}BM$ acceptor.[35] The *rre* PBDTTT-C-T based PSCs exhibited a PCE of 7.79%, which was much higher than that of the *rra* PBDTTT-C-T-based PSCs. Effective molecular ordering between the polymer chains of *rre* PBDTTT-C-T led to enhanced charge-carrier mobility and broader light absorption. The SCLC hole mobility ($\mu_{h,SCLC}$) of *rre* PBDTTT-C-T was 1.16×10^{-3} cm^2 V^{-1} s^{-1}, which is higher than that of *rra* PBDTTT-C-T (5.02×10^{-4} cm^2 V^{-1} s^{-1}). In addition, Bo *et al.* developed two P_Ds (*rre* PThE and *rra* PThE) consisting of benzodithiophene and ethyl 3-thiophenecarboxylate building blocks, which differed in terms of the directional RR, and employed them in the PSCs with ITTC NFSMAs.[30] While *rra* PThE yielded a PCE of 8.38%, *rre* PThE afforded a significantly increased PCE of 10.14%. Notably, the *rre* PThE:ITTC blends exhibited a higher $\mu_{h,SCLC}$ (5.24×10^{-5} cm^2 V^{-1} s^{-1}) than that of the *rra* PThE:ITTC blends (1.12×10^{-5} cm^2 V^{-1} s^{-1}). The same trends were also observed for other blends with other NFSMAs (*i.e.*, ITIC, and FTIC), where *rre* PThE afforded improved light absorption and charge-carrier mobilities of PThE-based PSCs. Thus, controlling the directional RR of D–A copolymers is important in optimizing the charge-carrier mobilities and PCEs of the PSCs.

3.2.2 Positional RR of D–A copolymers. Similar to directional RR, positional RR control also has a huge impact on the performance of PSCs. Many examples of polymers with positional RR control can be found in all-PSC systems, where many high-performance P_As are composed of either PDI or NDI derivatives with different positional RRs (Fig. 11 and Table 3). In 2018, Zhan *et al.* reported two regio-isomers of P(SePDI), where alternating selenophenes were attached to either 1,6- or 1,7-positions of PDI derivatives.[38] As shown in Fig. 11, the GIXS pattern of *rre*-P(SePDI) showed distinct scattering peaks along the out-of-plane direction, suggesting favorable face-on oriented molecular stacking within the film. In contrast, *rir*-P(SePDI) showed no scattering peaks, indicating an amorphous structure. The strong crystallinity of *rre*-P(SePDI) yielded a higher PCE of 6.2% and $\mu_{e,SCLC}$ of 5.4×10^{-4} cm^2 V^{-1} s^{-1} compared with those of *rir*-P(SePDI) (5.3% and 3.5×10^{-4} cm^2 V^{-1} s^{-1}, respectively). The impacts of positional RR control in NDI-based P_A were also investigated. Ludwigs *et al.* studied a series of P(NDIOD-T2) in which the positional RR ranged from 24 to 100%. *rre* P(NDIOD-T2) exhibited the highest $\mu_{e,SCLC}$ of 7×10^{-2} cm^2 V^{-1} s^{-1}, which was 10–100 times higher than that of *rir* P(NDIOD-T2). As presented above, the positionally *rre* CPs tend to result in a higher PCE in PSCs compared to the *rra* CPs. However, we note that strong aggregation of some of the highly *rre* CPs (*i.e.*, P(NDI2OD-T2)) can also induce severe phase separation in the BHJ that ultimately reduces the overall PCEs.[42]

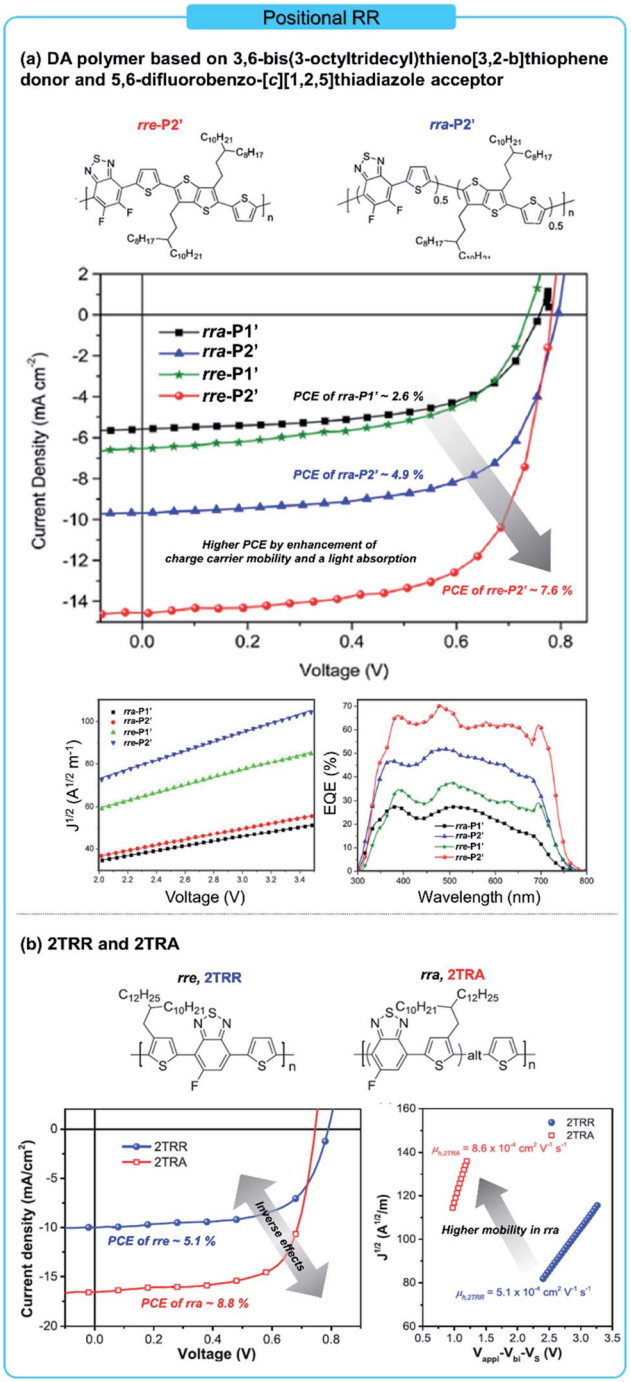

Fig. 12 Influences of RR on PCEs of PSCs based on D–A copolymers having different sequential RRs: (a) DA polymer based on 3,6-bis(3-octyltridecyl)thieno[3,2-b]thiophene donor and 5,6-difluorobenzo-[c][1,2,5]thiadiazole acceptor; and (b) 2TRR and 2TRA. Reproduced with permission.[45,48] Copyright 2016, American Chemical Society, and copyright 2017, Wiley.

Very recently, PSMAs have attracted significant attention as they combine the advantages of two distinct systems: (1) the strong light absorption and charge transport capability of NFSMAs,[159,160,186] and (2) the superior mechanical robustness and morphological stability of the polymeric active layers of all-PSCs.[5,151,154] Nevertheless, the PCE values of all-PSCs based on PSMAs remain lower than those of NFSMA-based PSCs. The lower PCEs are due, in part, to the inhomogeneous molecular structures with low positional RR of PSMAs.[40,41,167,169,170,187] To address these issues, He and co-workers recently demonstrated the importance of controlling the positional RR of the PSMAs. They first obtained isomerically pure monomers through recrystallization and employed them to achieve *rre* PBTIC-γ-2F2T PSMAs by polymerization (Fig. 11b).[167] The charge-carrier mobility of the resulting all-PSCs with *rre* PBTIC-γ-2F2T PSMAs was greatly enhanced and the voltage loss was greatly reduced, achieving a PCE of 14.34%. In contrast, the *rra* PBTIC-*m*-2F2T-based all-PSCs showed a PCE of only 3.26%. Moreover, Yang and co-workers reported *rre* PY-IT and *rre* PY-OT by polymerizing isomerically pure IC-Br(in) and IC-Br(out), respectively. The *rra* PY-IOT PSMAs comprising equal amounts of PY-IT and PY-OT were also compared.[39] The PY-IT-based PSCs afforded the best performance (PCE = 15.05%, Table 3) as a result of their stronger interchain interaction and optimized blend morphology with PM6 P_D. Interestingly, the PCE of the all-PSC device based on *rre* PY-OT PSMAs (10.04%) was lower than that of *rre* PY-IT, originating from deficient exciton dissociation, poor charge mobility, and severe charge recombination. These features were mainly driven from the curved molecular conformations of *rre* PY-OT PSMAs, which precluded the efficient formation of an intermolecular assembly. The *rra* PY-IOT PSMA-based devices exhibited an intermediate PCE of 12.12% where all photovoltaic parameters were between PY-IT and PY-OT. Thus, for the PSMA system, increasing the positional RR by using isomerically pure monomers is important. Also, controlling the molecular conformation by changing the positional RR of PSMAs is crucial for optimizing the properties of PSMAs and their performance in all-PSCs.[40,167,169,170,187]

3.2.3 Sequential RR of D–A copolymers. The control of sequential RR of CPs is crucial for both optoelectrical properties and high-performance PSCs (Fig. 12 and Table 4). As an example, *rra* and *rre* PDTSTTBDT D–A copolymers were produced by random-copolymerization with (D1–A1) and (D2–A2) dimers and self-condensation of (D1–A1–D2–A2) tetramers, respectively. The PSCs employing the *rre* PDTSTTBDT copolymers achieved higher PCEs than the *rra* PDTSTTBDT-based PSCs.[46] In addition, Ong and co-workers developed sequential RR-controlled D–A copolymers based on *rre* P2′ and *rra* P2′ (Fig. 12a). The *rre* P2′:$PC_{71}BM$ devices achieved a high PCE of 7.57% and $\mu_{h,SCLC}$ of 9.01×10^{-4} $cm^2\ V^{-1}\ s^{-1}$ compared to those of *rra* P2′:$PC_{71}BM$ (4.96% and 4.80×10^{-4} $cm^2\ V^{-1}\ s^{-1}$, respectively).[45] The improved molecular packing of *rre* polymers effectively enhances their charge-carrier mobility and light absorption properties. In the cases of PDTSTTBDT and difluorobenzene-NDI polymers with different arrangements of the sequence of repeating units (*i.e.*, P1′ and P2′ in Table 4), the *rre* polymers exhibited higher PCEs and SCLC mobilities than the *rra* polymers. However, sequentially *rre* polymers are not always beneficial for high performance PSCs. For example, Y. Cao *et al.* developed sequential RR-controlled polymers, 2TRR (*rre*) and 2TRA (*rra*).[48] The PCE and $\mu_{h,SCLC}$ of the *rra* 2TRA-based PSCs were higher (8.56% and 8.6×10^{-3} $cm^2\ V^{-1}\ s^{-1}$, respectively) than those of the *rre* 2TRR-based PSCs (5.05% and 5.1×10^{-4} $cm^2\ V^{-1}\ s^{-1}$, respectively) (Fig. 12b). More distributed alkyl chains within *rra* 2TRR afford localized aggregates and reduce the π–π stacking distance, increasing PCEs. In addition, Saeki *et al.* reported two sequential regio-isomers of *rre* PPy and *rra* PPy.[49] When blended with $PC_{71}BM$, *rra* PPy-based PSCs showed better PCE (3.75%) and $\mu_{h,SCLC}$ (9.1×10^{-6} $cm^2\ V^{-1}\ s^{-1}$) than *rre* PPy-based PSCs (2.56% and 6.4×10^{-6} $cm^2\ V^{-1}\ s^{-1}$, respectively). Therefore, the suitable control of sequential RR of CPs can further optimize the optoelectrical properties of the CPs as well as the PCE in PSCs. The structures of D–A copolymers described in this section and Tables 2–4 are shown in Fig. 13.

Table 4 PCEs of sequential *rre*- and *rra*-copolymer based PSCs

RR type	Active layer	RR	PCE [%]	$\mu_{h,SCLC}$ [$cm^2\ V^{-1}\ s^{-1}$]	$\mu_{e,SCLC}$ [$cm^2\ V^{-1}\ s^{-1}$]	Ref.
Sequential	***rre*-P1′**:$PC_{71}BM$	*rre*	3.59	5.80×10^{-4}	—	45
	***rra*-P1′**:$PC_{71}BM$	*rra*	2.60	3.49×10^{-4}	—	
	***rre*-P2′**:$PC_{71}BM$	*rre*	7.57	9.01×10^{-4}	—	
	***rra*-P2′**:$PC_{71}BM$	*rra*	4.96	4.80×10^{-4}	—	
	***rre* PDTSTTBDT**:$PC_{71}BM$	*rre*	6.14	7.0×10^{-5}	—	46
	***rra* PDTSTTBDT**:$PC_{71}BM$	*rra*	1.11	1.7×10^{-6}	—	
	PTB7-Th:**P2″**	*rre*	5.20	2.1×10^{-4}	1.6×10^{-4}	47
	PTB7-Th:**P1″**	*rra*	1.30	1.3×10^{-6}	7.3×10^{-5}	
	2TRR:$PC_{71}BM$	*rre*	5.05	5.1×10^{-4}[a]	—	48
	2TRA:$PC_{71}BM$	*rra*	8.56	8.6×10^{-3}[a]	—	
	***rre* PPy**:PCBM	*rre*	2.56	6.4×10^{-6}	2.1×10^{-4}	49
	***rra* PPy**:PCBM	*rra*	3.75	9.1×10^{-6}	8.5×10^{-4}	
	P1‴:PCBM	*rre*	0.45	—	—	50
	P2‴:PCBM	*rra*	2.30	—	—	
	P3‴:PCBM	*rra*	2.40	—	—	

[a] The mobility was measured with pristine polymer films (not blend).

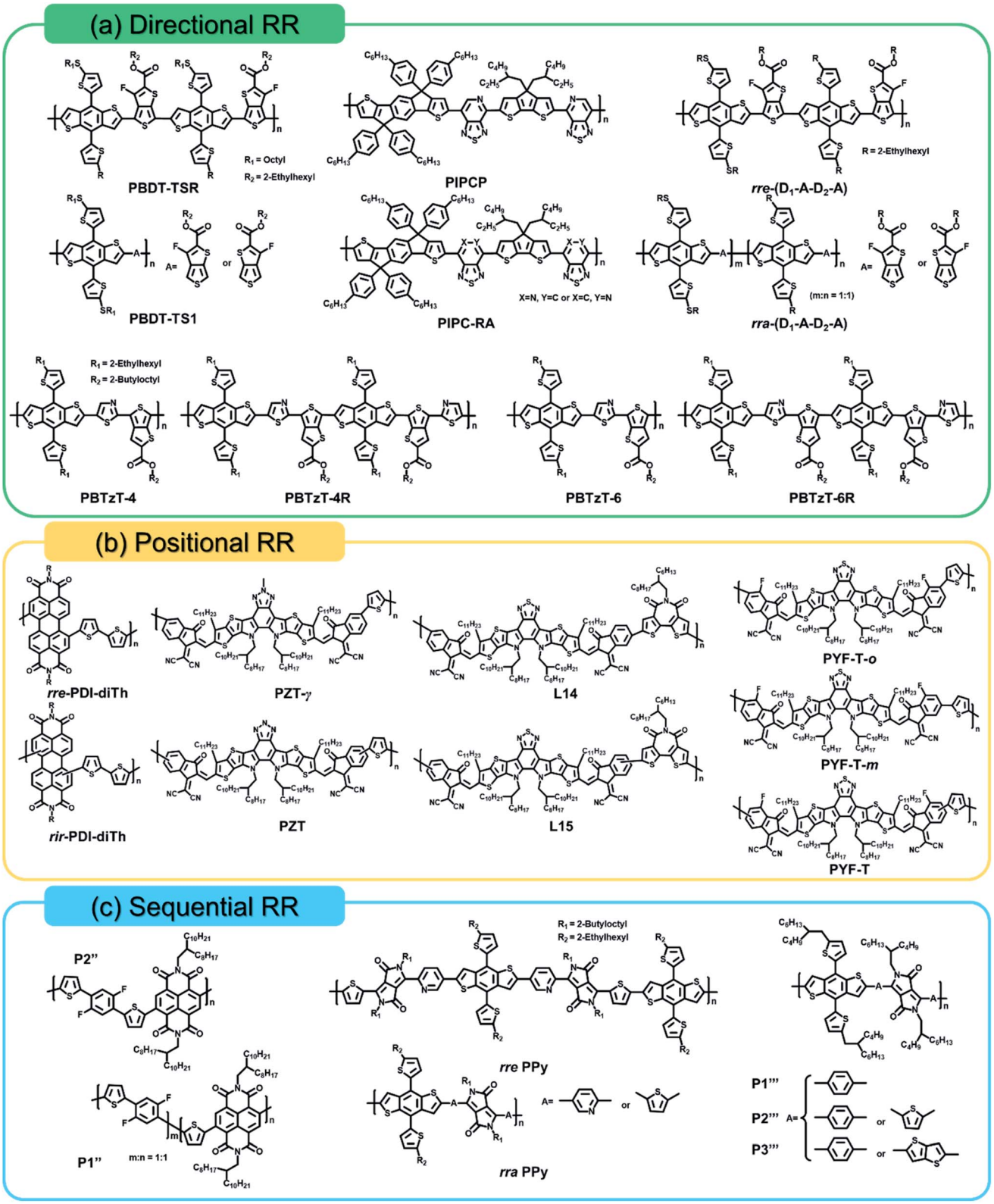

Fig. 13 Molecular structures of regioisomers in PSCs categorized by (a) directional RR, (b) positional RR, and (c) sequential RR which are described in Tables 2–4, respectively.

4. Conclusion and outlook

In this review, an overview of CPs with controlled RR, covering from simple homopolymers to state-of-the-art D–A copolymers, is presented. To provide a general guideline for RR control of a wide variety of CPs, we define three different types of RRs, *i.e.*, directional, positional and sequential RRs. We also highlight the importance of these three types of RRs from synthesis and properties of materials to performance of PSC devices.

The definition of RR for simple homopolymers with asymmetric alkyl chains such as P3ATs has been well-established. Also, various synthetic methods have been developed, which achieve the precise control of their structure and purity. As a result, the effect of the RR of CPs on the polymer properties and device performances has been extensively explored. In general, higher RR leads to stronger molecular interactions and higher crystallinity; thus, the optical and electrical properties can be enhanced to be suitable for the devices. However, the strong crystallization of high RR CPs can often induce low solution processability, mechanical fragility, and low thermal stability in PSC blends. Therefore, precise RR control is important in the design of CPs for various organic electronic applications.

While the importance of the RR of homopolymers is relatively well-demonstrated, the RR of recently developed high-performance CPs such as D–A copolymers and PSMA has largely been unexplored due to their chemical complexity and lack of synthetic methods to control RR. However, since the state-of-the-art device performances are achieved by the D–A copolymers and PSMA, controlling the RR of these CPs is emerging as a crucial parameter for high-performance materials. From many examples of these CPs, we categorize the RR-varied polymers into three types depending on the directional, positional, and sequential regularities of the repeating units. Then, we describe synthetic methods to control each type of RR, and its impact on the optoelectrical properties of the polymers and their device performances. In directional RR, regular alignments of the functional groups and/or side chains in the same direction induces stronger molecular packing and enhanced optoelectrical properties, improving device performances compared to those afforded by the random isomers. Different positional RR induces changes in the molecular conformation due to the different tilted angles between the repeating units of the CPs. Therefore, control of positional RR can give rise to unique crystal structures. Positionally *rre* CPs generally exhibit excellent optoelectrical properties and enhanced performances in PSCs. Compared with directional and positional RR, differences in sequential RR induce larger impacts on the optoelectrical properties of the CPs. Sequentially *rre* CPs typically are more crystalline. Nevertheless, some examples show that sequentially *rir* CPs can result in a higher PCE of the PSCs, probably due to the inferior morphology of the *rre* CP-based blends driven by excessive crystallization. Therefore, delicate tuning of the sequential RR is required for achieving high-performance PSCs.

The importance of controlling the RR of D–A copolymers has been recently highlighted in the organic electronics community. Many unrevealed correlations between the RR of D–A copolymers and their properties/device performances should be elucidated. For example, tuning the mechanical properties of CPs without compromising their electrical and optical properties is of great importance for their applications in wearable and portable electronics. While RR is one of the key parameters for controlling the mechanical properties of the polymers, the impact of the RR control is largely unexplored for the high-performance D–A copolymers. Most examples of RR-controlled polymers have been found in the PSC and organic transistor applications and the studies should be extended to other electronic devices considering the huge influence of RR on various intrinsic properties of CPs.

Conflicts of interest

There are no conflicts to declare.

Acknowledgements

This work was supported by the National Research Foundation of Korea (2017M3D1A1039553 and 2020R1A4A1018516). This research is additionally performed as a cooperation project of "Basic project", supported by the Korea Research Institute of Chemical Technology (KRICT). And, this work is also supported by (Grant No. 1425144083) the Ministry of SMEs and Startups of the Korean Government.

References

1 C. Bruner and R. Dauskardt, *Macromolecules*, 2014, **47**, 1117–1121.
2 N. B. Kolhe, D. K. Tran, H. Lee, D. Kuzuhara, N. Yoshimoto, T. Koganezawa and S. A. Jenekhe, *ACS Energy Lett.*, 2019, **4**, 1162–1170.
3 J. Chen, X. Zhuang, W. Huang, M. Su, L.-w. Feng, S. M. Swick, G. Wang, Y. Chen, J. Yu, X. Guo, T. J. Marks and A. Facchetti, *Chem. Mater.*, 2020, **32**, 5317–5326.
4 S. Samal and B. C. Thompson, *ACS Macro Lett.*, 2018, **7**, 1161–1167.
5 C. Lee, S. Lee, G.-U. Kim, W. Lee and B. J. Kim, *Chem. Rev.*, 2019, **119**, 8028–8086.
6 Y. Zhang, D. Hanifi, E. Lim, S. Chourou, S. Alvarez, A. Pun, A. Hexemer, B. Ma and Y. Liu, *Adv. Mater.*, 2014, **26**, 1223–1228.
7 M. Kim, S. U. Ryu, S. A. Park, K. Choi, T. Kim, D. Chung and T. Park, *Adv. Funct. Mater.*, 2020, **30**, 1904545.
8 J. Z. Low, B. Capozzi, J. Cui, S. Wei, L. Venkataraman and L. M. Campos, *Chem. Sci.*, 2017, **8**, 3254–3259.
9 M. Kim, H. I. Kim, S. U. Ryu, S. Y. Son, S. A. Park, N. Khan, W. S. Shin, C. E. Song and T. Park, *Chem. Mater.*, 2019, **31**, 5047–5055.
10 S.-I. Na, Y.-H. Seo, Y.-C. Nah, S.-S. Kim, H. Heo, J.-E. Kim, N. Rolston, R. H. Dauskardt, M. Gao, Y. Lee and D. Vak, *Adv. Funct. Mater.*, 2019, **29**, 1805825.

11 N. B. Kolhe, H. Lee, D. Kuzuhara, N. Yoshimoto, T. Koganezawa and S. A. Jenekhe, *Chem. Mater.*, 2018, **30**, 6540–6548.
12 Y.-J. Hwang, H. Li, B. A. E. Courtright, S. Subramaniyan and S. A. Jenekhe, *Adv. Mater.*, 2016, **28**, 124–131.
13 Y. Wang, T. Hasegawa, H. Matsumoto and T. Michinobu, *J. Am. Chem. Soc.*, 2019, **141**, 3566–3575.
14 E. Wang, W. Mammo and M. R. Andersson, *Adv. Mater.*, 2014, **26**, 1801–1826.
15 A. X. Chen, A. T. Kleinschmidt, K. Choudhary and D. J. Lipomi, *Chem. Mater.*, 2020, **32**, 7582–7601.
16 E. L. Melenbrink, K. M. Hilby, K. Choudhary, S. Samal, N. Kazerouni, J. L. McConn, D. J. Lipomi and B. C. Thompson, *ACS Appl. Mater. Interfaces*, 2019, **1**, 1107–1117.
17 S. W. Kim, Y. Wang, H. You, W. Lee, T. Michinobu and B. J. Kim, *ACS Appl. Mater. Interfaces*, 2019, **11**, 35896–35903.
18 R. Ma, T. Liu, Z. Luo, K. Gao, K. Chen, G. Zhang, W. Gao, Y. Xiao, T.-K. Lau, Q. Fan, Y. Chen, L.-K. Ma, H. Sun, G. Cai, T. Yang, X. Lu, E. Wang, C. Yang, A. K. Y. Jen and H. Yan, *ACS Energy Lett.*, 2020, **5**, 2711–2720.
19 L. Ying, F. Huang and G. C. Bazan, *Nat. Commun.*, 2017, **8**, 14047.
20 I. Osaka and R. D. McCullough, *Acc. Chem. Res.*, 2008, **41**, 1202–1214.
21 B. Amna, H. M. Siddiqi, A. Hassan and T. Ozturk, *RSC Adv.*, 2020, **10**, 4322–4396.
22 B. Kuei and E. D. Gomez, *Soft Matter*, 2017, **13**, 49–67.
23 A. R. Aiyar, J.-I. Hong and E. Reichmanis, *Chem. Mater.*, 2012, **24**, 2845–2853.
24 C. R. Snyder and E. D. Gomez, *J. Polym. Sci., Part B: Polym. Phys.*, 2016, **54**, 1202–1206.
25 J.-S. Kim, J.-H. Kim, W. Lee, H. Yu, H. J. Kim, I. Song, M. Shin, J. H. Oh, U. Jeong and T.-S. Kim, *Macromolecules*, 2015, **48**, 4339–4346.
26 M. Baghgar, J. Labastide, F. Bokel, I. Dujovne, A. McKenna, A. M. Barnes, E. Pentzer, T. Emrick, R. Hayward and M. D. Barnes, *J. Phys. Chem. Lett.*, 2012, **3**, 1674–1679.
27 P. Kohn, S. Huettner, H. Komber, V. Senkovskyy, R. Tkachov, A. Kiriy, R. H. Friend, U. Steiner, W. T. S. Huck, J.-U. Sommer and M. Sommer, *J. Am. Chem. Soc.*, 2012, **134**, 4790–4805.
28 S. Pankaj, E. Hempel and M. Beiner, *Macromolecules*, 2009, **42**, 716–724.
29 S. Qu, C. Ming, Q. Yao, W. Lu, K. Zeng, W. Shi, X. Shi, C. Uher and L. Chen, *Polymers*, 2018, **10**, 815.
30 Y. Liu, H. Lu, M. Li, Z. Zhang, S. Feng, X. Xu, Y. Wu and Z. Bo, *Macromolecules*, 2018, **51**, 8646–8651.
31 H. Yao, W. Zhao, Z. Zheng, Y. Cui, J. Zhang, Z. Wei and J. Hou, *J. Mater. Chem. A*, 2016, **4**, 1708–1713.
32 S. W. Kim, H. Kim, J.-W. Lee, C. Lee, B. Lim, J. Lee, Y. Lee and B. J. Kim, *Macromolecules*, 2019, **52**, 738–746.
33 M. Wang, H. Wang, T. Yokoyama, X. Liu, Y. Huang, Y. Zhang, T.-Q. Nguyen, S. Aramaki and G. C. Bazan, *J. Am. Chem. Soc.*, 2014, **136**, 12576–12579.
34 D. Zhu, Q. Wang, Y. Wang, X. Bao, M. Qiu, B. Shahid, Y. Li and R. Yang, *Chem. Mater.*, 2018, **30**, 4639–4645.
35 H. Kim, H. Lee, D. Seo, Y. Jeong, K. Cho, J. Lee and Y. Lee, *Chem. Mater.*, 2015, **27**, 3102–3107.
36 H. Zhong, L. Ye, J.-Y. Chen, S. B. Jo, C.-C. Chueh, J. H. Carpenter, H. Ade and A. K. Y. Jen, *J. Mater. Chem. A*, 2017, **5**, 10517–10525.
37 Y. Zhou, Q. Yan, Y.-Q. Zheng, J.-Y. Wang, D. Zhao and J. Pei, *J. Mater. Chem. A*, 2013, **1**, 6609–6613.
38 Y. Liang, S. Lan, P. Deng, D. Zhou, Z. Guo, H. Chen and H. Zhan, *ACS Appl. Mater. Interfaces*, 2018, **10**, 32397–32403.
39 Z. Luo, T. Liu, R. Ma, Y. Xiao, L. Zhan, G. Zhang, H. Sun, F. Ni, G. Chai, J. Wang, C. Zhong, Y. Zou, X. Guo, X. Lu, H. Chen, H. Yan and C. Yang, *Adv. Mater.*, 2020, **32**, 2005942.
40 H. Yu, M. Pan, R. Sun, I. Agunawela, J. Zhang, Y. Li, Z. Qi, H. Han, X. Zou, W. Zhou, S. Chen, J. Y. L. Lai, S. Luo, Z. Luo, D. Zhao, X. Lu, H. Ade, F. Huang, J. Min and H. Yan, *Angew. Chem., Int. Ed.*, 2021, **60**, 10137–10146.
41 H. Fu, Y. Li, J. Yu, Z. Wu, Q. Fan, F. Lin, H. Y. Woo, F. Gao, Z. Zhu and A. K. Y. Jen, *J. Am. Chem. Soc.*, 2021, **143**, 2665–2670.
42 Y. M. Gross, D. Trefz, R. Tkachov, V. Untilova, M. Brinkmann, G. L. Schulz and S. Ludwigs, *Macromolecules*, 2017, **50**, 5353–5366.
43 R. Steyrleuthner, R. Di Pietro, B. A. Collins, F. Polzer, S. Himmelberger, M. Schubert, Z. Chen, S. Zhang, A. Salleo, H. Ade, A. Facchetti and D. Neher, *J. Am. Chem. Soc.*, 2014, **136**, 4245–4256.
44 S. Wang, D. Fazzi, Y. Puttisong, M. J. Jafari, Z. Chen, T. Ederth, J. W. Andreasen, W. M. Chen, A. Facchetti and S. Fabiano, *Chem. Mater.*, 2019, **31**, 3395–3406.
45 P. Deng, B. Wu, Y. Lei, H. Cao and B. S. Ong, *Macromolecules*, 2016, **49**, 2541–2548.
46 H. Heo, H. Kim, D. Lee, S. Jang, L. Ban, B. Lim, J. Lee and Y. Lee, *Macromolecules*, 2016, **49**, 3328–3335.
47 P. Deng, C. H. Y. Ho, Y. Lu, H.-W. Li, S.-W. Tsang, S. K. So and B. S. Ong, *Commun. Chem.*, 2017, **53**, 3249–3252.
48 C. Zhou, Z. Chen, G. Zhang, C. McDowell, P. Luo, X. Jia, M. J. Ford, M. Wang, G. C. Bazan, F. Huang and Y. Cao, *Adv. Energy Mater.*, 2018, **8**, 1701668.
49 K. Aoshima, M. Nomura and A. Saeki, *ACS Omega*, 2019, **4**, 15645–15652.
50 K. Aoshima, M. Ide and A. Saeki, *RSC Adv.*, 2018, **8**, 30201–30206.
51 M. Kobayashi, J. Chen, T. C. Chung, F. Moraes, A. J. Heeger and F. Wudl, *Synth. Met.*, 1984, **9**, 77–86.
52 R. D. McCullough and S. P. Williams, *J. Am. Chem. Soc.*, 1993, **115**, 11608–11609.
53 R. L. Elsenbaumer, K. Y. Jen and R. Oboodi, *Synth. Met.*, 1986, **15**, 169–174.
54 R. S. Maior, K. Hinkelmann, H. Eckert and F. Wudl, *Macromolecules*, 1990, **23**, 1268–1279.
55 M. Leclerc, F. M. Diaz and G. Wegner, *Makromol. Chem.*, 1989, **190**, 3105–3116.

56 S. Amou, O. Haba, K. Shirato, T. Hayakawa, M. Ueda, K. Takeuchi and M. Asai, *J. Polym. Sci., Part A: Polym. Chem.*, 1999, **37**, 1943–1948.
57 R. D. Mccullough, S. P. Williams, S. Tristramnagle, M. Jayaraman, P. C. Ewbank and L. Miller, *Synth. Met.*, 1995, **69**, 279–282.
58 R. D. Mccullough, R. D. Lowe, M. Jayaraman and D. L. Anderson, *J. Org. Chem.*, 1993, **58**, 904–912.
59 R. D. Mccullough, S. Tristramnagle, S. P. Williams, R. D. Lowe and M. Jayaraman, *J. Am. Chem. Soc.*, 1993, **115**, 4910–4911.
60 R. D. Mccullough, R. D. Lowe, M. Jayaraman and D. L. Anderson, *J. Org. Chem.*, 1993, **58**, 904–912.
61 T. A. Chen, X. M. Wu and R. D. Rieke, *J. Am. Chem. Soc.*, 1995, **117**, 233–244.
62 T. A. Chen and R. D. Rieke, *J. Am. Chem. Soc.*, 1992, **114**, 10087–10088.
63 R. S. Loewe, S. M. Khersonsky and R. D. McCullough, *Adv. Mater.*, 1999, **11**, 250–253.
64 E. E. Sheina, J. S. Liu, M. C. Iovu, D. W. Laird and R. D. McCullough, *Macromolecules*, 2004, **37**, 3526–3528.
65 R. Miyakoshi, A. Yokoyama and T. Yokozawa, *J. Am. Chem. Soc.*, 2005, **127**, 17542–17547.
66 M. Jeffries-El, G. Sauve and R. D. McCullough, *Adv. Mater.*, 2004, **16**, 1017–1019.
67 M. Jeffries-El, G. Sauve and R. D. McCullough, *Macromolecules*, 2005, **38**, 10346–10352.
68 H. C. Moon, D. Bae and J. K. Kim, *Macromolecules*, 2012, **45**, 5201–5207.
69 V. Ho, B. W. Boudouris, B. L. McCulloch, C. G. Shuttle, M. Burkhardt, M. L. Chabinyc and R. A. Segalman, *J. Am. Chem. Soc.*, 2011, **133**, 9270–9273.
70 G. Barker, *J. Mater. Chem.*, 1998, **8**, 25–29.
71 S. Guillerez and G. Bidan, *Synth. Met.*, 1998, **93**, 123–126.
72 Y. Qiu, J. C. Worch, A. Fortney, C. Gayathri, R. R. Gil and K. J. T. Noonan, *Macromolecules*, 2016, **49**, 4757.
73 B. C. Thompson, B. J. Kim, D. F. Kavulak, K. Sivula, C. Mauldin and J. M. J. Fréchet, *Macromolecules*, 2007, **40**, 7425–7428.
74 J.-S. Kim, J.-E. Choi, H. Park, Y. Kim, H. J. Kim, J. Han, J. M. Shin and B. J. Kim, *Polym. Chem.*, 2019, **10**, 3030–3039.
75 T. Menda, T. Mori and T. Yasuda, *Polym. J.*, 2021, **53**, 403–408.
76 N. S. Gobalasingham, S. Noh and B. C. Thompson, *Polym. Chem.*, 2016, **7**, 1623.
77 B. McCulloch, V. Ho, M. Hoarfrost, C. Stanley, C. Do, W. T. Heller and R. A. Segalman, *Macromolecules*, 2013, **46**, 1899–1907.
78 P. Willot, J. Steverlynck, D. Moerman, P. Leclere, R. Lazzaroni and G. Koeckelberghs, *Polym. Chem.*, 2013, **4**, 2662–2671.
79 T. Adachi, J. Brazard, R. J. Ono, B. Hanson, M. C. Traub, Z. Q. Wu, Z. C. Li, J. C. Bolinger, V. Ganesan, C. W. Bielawski, D. A. V. Bout and P. F. Barbara, *J. Phys. Chem. Lett.*, 2011, **2**, 1400–1404.
80 S. Pal and A. K. Nandi, *Macromolecules*, 2003, **36**, 8426–8432.
81 H. Sirringhaus, P. J. Brown, R. H. Friend, M. M. Nielsen, K. Bechgaard, B. M. W. Langeveld-Voss, A. J. H. Spiering, R. A. J. Janssen, E. W. Meijer, P. Herwig and D. M. de Leeuw, *Nature*, 1999, **401**, 685–688.
82 K. Zhou, J. G. Liu, R. Zhang, Q. Q. Zhao, X. X. Cao, X. H. Yu, R. B. Xing and Y. C. Han, *Polymer*, 2016, **86**, 105–112.
83 C. H. Woo, B. C. Thompson, B. J. Kim, M. F. Toney and J. M. J. Frechet, *J. Am. Chem. Soc.*, 2008, **130**, 16324–16329.
84 L. Qiu, W. H. Lee, X. Wang, J. S. Kim, J. A. Lim, D. Kwak, S. Lee and K. Cho, *Adv. Mater.*, 2009, **21**, 1349–1353.
85 K. A. Mazzio, A. H. Rice, M. M. Durban and C. K. Luscombe, *J. Phys. Chem. C*, 2015, **119**, 14911–14918.
86 H. J. Kim, J.-S. Kim, Y. Kim, Y. S. Jung, B. J. Kim and Y. Kim, *Polymer*, 2019, **178**, 121569.
87 J.-S. Kim, J. Han, Y. Kim, H. Park, J. P. Coote, G. E. Stein and B. J. Kim, *Macromolecules*, 2018, **51**, 4077–4084.
88 J.-S. Kim, Y. Kim, H.-J. Kim, H. J. Kim, H. Yang, Y. S. Jung, G. E. Stein and B. J. Kim, *Macromolecules*, 2017, **50**, 1902–1908.
89 Y. Kim, H. J. Kim, J.-S. Kim, H. Yun, H. Park, J. Han and B. J. Kim, *Chem. Mater.*, 2018, **30**, 7912–7921.
90 C. A. Sandstedt, R. D. Rieke and C. J. Eckhardt, *Chem. Mater.*, 1995, **7**, 1057–1059.
91 P. J. Brown, D. S. Thomas, A. Kohler, J. S. Wilson, J. S. Kim, C. M. Ramsdale, H. Sirringhaus and R. H. Friend, *Phys. Rev. B: Condens. Matter Mater. Phys.*, 2003, **67**, 064203.
92 L. Brambilla, J. S. Kim, B. J. Kim, V. Hernandez, J. T. L. Navarrete and G. Zerbi, *J. Mol. Struct.*, 2020, **1221**, 128882.
93 J. Clark, J.-F. Chang, F. C. Spano, R. H. Friend and C. Silva, *Appl. Phys. Lett.*, 2009, **94**, 163306.
94 C. Carach, I. Riisness and M. J. Gordon, *Appl. Phys. Lett.*, 2012, **101**, 083302.
95 O. J. Korovyanko, R. Osterbacka, X. M. Jiang, Z. V. Vardeny and R. A. J. Janssen, *Phys. Rev. B: Condens. Matter Mater. Phys.*, 2001, **64**, 235122.
96 R. Mauer, M. Kastler and F. Laquai, *Adv. Funct. Mater.*, 2010, **20**, 2085–2092.
97 F. C. Grozema, P. T. van Duijnen, Y. A. Berlin, M. A. Ratner and L. D. A. Siebbeles, *J. Phys. Chem. B*, 2002, **106**, 7791–7795.
98 C. Poelking and D. Andrienko, *Macromolecules*, 2013, **46**, 8941–8956.
99 W. Takashima, S. S. Pandey, T. Endo, M. Rikukawa and K. Kaneto, *Curr. Appl. Phys.*, 2001, **1**, 90–97.
100 D. H. Kim, J. T. Han, Y. D. Park, Y. Jang, J. H. Cho, M. Hwang and K. Cho, *Adv. Mater.*, 2006, **18**, 719–723.
101 S. K. Patra, R. Ahmed, G. R. Whittell, D. J. Lunn, E. L. Dunphy, M. A. Winnik and I. Manners, *J. Am. Chem. Soc.*, 2011, **133**, 8842–8845.
102 C. Yang, J. K. Lee, A. J. Heeger and F. Wudl, *J. Mater. Chem.*, 2009, **19**, 5416–5423.
103 E. J. W. Crossland, K. Tremel, F. Fischer, K. Rahimi, G. Reiter, U. Steiner and S. Ludwigs, *Adv. Mater.*, 2012, **24**, 839–844.
104 P.-T. Wu, H. Xin, F. S. Kim, G. Ren and S. A. Jenekhe, *Macromolecules*, 2009, **42**, 8817–8826.

105 A. D. Printz and D. J. Lipomi, *Appl. Phys. Rev.*, 2016, **3**, 021302.
106 G.-J. N. Wang, A. Gasperini and Z. Bao, *Adv. Electron. Mater.*, 2018, **4**, 1700429.
107 H.-C. Wu, S. J. Benight, A. Chortos, W.-Y. Lee, J. Mei, J. W. F. To, C. Lu, M. He, J. B. H. Tok, W.-C. Chen and Z. Bao, *Chem. Mater.*, 2014, **26**, 4544–4551.
108 R. Peng, B. Pang, D. Hu, M. Chen, G. Zhang, X. Wang, H. Lu, K. Cho and L. Qiu, *J. Mater. Chem. C*, 2015, **3**, 3599–3606.
109 Z. C. Smith, Z. M. Wright, A. M. Arnold, G. Sauvé, R. D. McCullough and S. A. Sydlik, *Adv. Electron. Mater.*, 2017, **3**, 1600316.
110 J. I. Scott, X. Xue, M. Wang, R. J. Kline, B. C. Hoffman, D. Dougherty, C. Zhou, G. Bazan and B. T. O'Connor, *ACS Appl. Mater. Interfaces*, 2016, **8**, 14037–14045.
111 D. Choi, H. Kim, N. Persson, P.-H. Chu, M. Chang, J.-H. Kang, S. Graham and E. Reichmanis, *Chem. Mater.*, 2016, **28**, 1196–1204.
112 J. Xu, S. Wang, G. Wang, C. Zhu, S. Luo, L. Jin, X. Gu, S. Chen, V. R. Feig, J. W. F. To, S. Rondeau-Gagné, J. Park, B. Schroeder, C. Lu, J. Y. Oh, Y. Wang, Y.-H. Kim, H. Yan, R. Sinclair, D. Zhou, G. Xue, B. Murmann, C. Linder, W. Cai, J. B.-H. Tok, J. W. Chung and Z. Bao, *Science*, 2017, **355**, 59–64.
113 D. J. Lipomi, B. C. K. Tee, M. Vosgueritchian and Z. Bao, *Adv. Mater.*, 2011, **23**, 1771–1775.
114 H. Park, B. S. Ma, J. S. Kim, Y. Kim, H. J. Kim, D. Kim, H. Yun, J. Han, F. S. Kim, T. S. Kim and B. J. Kim, *Macromolecules*, 2019, **52**, 7721–7730.
115 H. J. Kim, M. Y. Lee, J. S. Kim, J. H. Kim, H. Yu, H. Yun, K. Liao, T. S. Kim, J. H. Oh and B. J. Kim, *ACS Appl. Mater. Interfaces*, 2017, **9**, 14120–14128.
116 P. H. Chu, G. Wang, B. Y. Fu, D. Choi, J. O. Park, M. Srinivasarao and E. Reichmanis, *Adv. Electron. Mater.*, 2016, **2**, 1500384.
117 H. Sun, B. Liu, Y. Ma, J.-W. Lee, J. Yang, J. Wang, Y. Li, B. Li, K. Feng, Y. Shi, B. Zhang, D. Han, H. Meng, L. Niu, B. J. Kim, Q. Zheng and X. Guo, *Adv. Mater.*, 2021, **33**, 2102635.
118 S. Seo, C. Sun, J.-W. Lee, S. Lee, D. Lee, C. Wang, T. N.-L. Phan, G.-U. Kim, S. Cho, Y.-H. Kim and B. J. Kim, *Adv. Funct. Mater.*, 2021, 2108508.
119 K.-H. Kim, S. Park, H. Yu, H. Kang, I. Song, J. H. Oh and B. J. Kim, *Chem. Mater.*, 2014, **26**, 6963–6970.
120 T. E. Kang, K.-H. Kim and B. J. Kim, *J. Mater. Chem. A*, 2014, **2**, 15252–15267.
121 T. E. Kang, H.-H. Cho, H. j. Kim, W. Lee, H. Kang and B. J. Kim, *Macromolecules*, 2013, **46**, 6806–6813.
122 Z. Genene, J. Wang, X. Xu, R. Yang, W. Mammo and E. Wang, *RSC Adv.*, 2017, **7**, 17959–17967.
123 D. Chen, S. Liu, J. Liu, J. Han, L. Chen and Y. Chen, *ACS Appl. Mater. Interfaces*, 2021, **3**, 1923–1931.
124 D. Dang, D. Yu and E. Wang, *Adv. Mater.*, 2019, **31**, 1807019.
125 J. Wu, G. Li, J. Fang, X. Guo, L. Zhu, B. Guo, Y. Wang, G. Zhang, L. Arunagiri, F. Liu, H. Yan, M. Zhang and Y. Li, *Nat. Commun.*, 2020, **11**, 4612.
126 O. Inganäs, *Adv. Mater.*, 2018, **30**, 1800388.
127 P. P. Khlyabich, M. Sezen-Edmonds, J. B. Howard, B. C. Thompson and Y.-L. Loo, *ACS Energy Lett.*, 2017, **2**, 2149–2156.
128 B. C. Thompson and J. M. J. Fréchet, *Angew. Chem., Int. Ed.*, 2008, **47**, 58–77.
129 B. Kippelen and J.-L. Brédas, *Energy Environ. Sci.*, 2009, **2**, 251–261.
130 K. A. Mazzio and C. K. Luscombe, *Chem. Soc. Rev.*, 2015, **44**, 78–90.
131 C. J. Brabec, S. Gowrisanker, J. J. M. Halls, D. Laird, S. Jia and S. P. Williams, *Adv. Mater.*, 2010, **22**, 3839–3856.
132 Z. Luo, R. Ma, T. Liu, J. Yu, Y. Xiao, R. Sun, G. Xie, J. Yuan, Y. Chen, K. Chen, G. Chai, H. Sun, J. Min, J. Zhang, Y. Zou, C. Yang, X. Lu, F. Gao and H. Yan, *Joule*, 2020, **4**, 1236–1247.
133 L. Zhan, S. Li, T.-K. Lau, Y. Cui, X. Lu, M. Shi, C.-Z. Li, H. Li, J. Hou and H. Chen, *Energy Environ. Sci.*, 2020, **13**, 635–645.
134 Y. Lin, J. Wang, Z.-G. Zhang, H. Bai, Y. Li, D. Zhu and X. Zhan, *Adv. Mater.*, 2015, **27**, 1170–1174.
135 S. Zhang, Y. Qin, J. Zhu and J. Hou, *Adv. Mater.*, 2018, **30**, 1800868.
136 C. Sun, F. Pan, H. Bin, J. Zhang, L. Xue, B. Qiu, Z. Wei, Z.-G. Zhang and Y. Li, *Nat. Commun.*, 2018, **9**, 743.
137 V. Vohra, K. Kawashima, T. Kakara, T. Koganezawa, I. Osaka, K. Takimiya and H. Murata, *Nat. Photonics*, 2015, **9**, 403–408.
138 G. Wang, F. S. Melkonyan, A. Facchetti and T. J. Marks, *Angew. Chem., Int. Ed.*, 2019, **58**, 4129–4142.
139 A. Facchetti, *Mater. Today*, 2013, **16**, 123–132.
140 Z. Genene, W. Mammo, E. Wang and M. R. Andersson, *Adv. Mater.*, 2019, **31**, 1807275.
141 Z. Li, L. Ying, P. Zhu, W. Zhong, N. Li, F. Liu, F. Huang and Y. Cao, *Energy Environ. Sci.*, 2019, **12**, 157–163.
142 R. Zhao, N. Wang, Y. Yu and J. Liu, *Chem. Mater.*, 2020, **32**, 1308–1314.
143 Y.-J. Hwang, B. A. E. Courtright, A. S. Ferreira, S. H. Tolbert and S. A. Jenekhe, *Adv. Mater.*, 2015, **27**, 4578–4584.
144 H. Yao, F. Bai, H. Hu, L. Arunagiri, J. Zhang, Y. Chen, H. Yu, S. Chen, T. Liu, J. Y. L. Lai, Y. Zou, H. Ade and H. Yan, *ACS Energy Lett.*, 2019, **4**, 417–422.
145 H. Sun, B. Liu, C. W. Koh, Y. Zhang, J. Chen, Y. Wang, P. Chen, B. Tu, M. Su, H. Wang, Y. Tang, Y. Shi, H. Y. Woo and X. Guo, *Adv. Funct. Mater.*, 2019, **29**, 1903970.
146 S. Chen, Y. An, G. K. Dutta, Y. Kim, Z.-G. Zhang, Y. Li and C. Yang, *Adv. Funct. Mater.*, 2017, **27**, 1603564.
147 J.-W. Lee, C. Sun, B. S. Ma, H. J. Kim, C. Wang, J. M. Ryu, C. Lim, T.-S. Kim, Y.-H. Kim, S.-K. Kwon and B. J. Kim, *Adv. Energy Mater.*, 2021, **11**, 2003367.
148 R. Zhao, J. Liu and L. Wang, *Acc. Chem. Res.*, 2020, **53**, 1557–1567.
149 D. K. Tran, A. Robitaille, I. J. Hai, X. Ding, D. Kuzuhara, T. Koganezawa, Y.-C. Chiu, M. Leclerc and S. A. Jenekhe, *J. Mater. Chem. A*, 2020, **8**, 21070–21083.
150 H. Benten, T. Nishida, D. Mori, H. Xu, H. Ohkita and S. Ito, *Energy Environ. Sci.*, 2016, **9**, 135–140.
151 H. Kang, W. Lee, J. Oh, T. Kim, C. Lee and B. J. Kim, *Acc. Chem. Res.*, 2016, **49**, 2424–2434.

152 T. Kim, J.-H. Kim, T. E. Kang, C. Lee, H. Kang, M. Shin, C. Wang, B. Ma, U. Jeong, T.-S. Kim and B. J. Kim, *Nat. Commun.*, 2015, **6**, 8547.
153 P. B. J. St. Onge, M. U. Ocheje, M. Selivanova and S. Rondeau-Gagné, *Chem. Rec.*, 2019, **19**, 1008–1027.
154 N. Balar, J. J. Rech, R. Henry, L. Ye, H. Ade, W. You and B. T. O'Connor, *Chem. Mater.*, 2019, **31**, 5124–5132.
155 J. Choi, W. Kim, S. Kim, T.-S. Kim and B. J. Kim, *Chem. Mater.*, 2019, **31**, 9057–9069.
156 Q. Fan, W. Su, S. Chen, W. Kim, X. Chen, B. Lee, T. Liu, U. A. Méndez-Romero, R. Ma, T. Yang, W. Zhuang, Y. Li, Y. Li, T.-S. Kim, L. Hou, C. Yang, H. Yan, D. Yu and E. Wang, *Joule*, 2020, **4**, 658–672.
157 F. P. V. Koch, J. Rivnay, S. Foster, C. Müller, J. M. Downing, E. Buchaca-Domingo, P. Westacott, L. Yu, M. Yuan, M. Baklar, Z. Fei, C. Luscombe, M. A. McLachlan, M. Heeney, G. Rumbles, C. Silva, A. Salleo, J. Nelson, P. Smith and N. Stingelin, *Prog. Polym. Sci.*, 2013, **38**, 1978–1989.
158 Y. Wang, J. Lee, X. Hou, C. Labanti, J. Yan, E. Mazzolini, A. Parhar, J. Nelson, J.-S. Kim and Z. Li, *Adv. Energy Mater.*, 2021, **11**, 2003002.
159 S. Li, C.-Z. Li, M. Shi and H. Chen, *ACS Energy Lett.*, 2020, **5**, 1554–1567.
160 C. Yan, S. Barlow, Z. Wang, H. Yan, A. K. Y. Jen, S. R. Marder and X. Zhan, *Nat. Rev. Mater.*, 2018, **3**, 18003.
161 Y. Cui, H. Yao, J. Zhang, K. Xian, T. Zhang, L. Hong, Y. Wang, Y. Xu, K. Ma, C. An, C. He, Z. Wei, F. Gao and J. Hou, *Adv. Mater.*, 2020, **32**, 1908205.
162 J. Yuan, Y. Zhang, L. Zhou, G. Zhang, H.-L. Yip, T.-K. Lau, X. Lu, C. Zhu, H. Peng, P. A. Johnson, M. Leclerc, Y. Cao, J. Ulanski, Y. Li and Y. Zou, *Joule*, 2019, **3**, 1140–1151.
163 Q. Liu, Y. Jiang, K. Jin, J. Qin, J. Xu, W. Li, J. Xiong, J. Liu, Z. Xiao, K. Sun, S. Yang, X. Zhang and L. Ding, *Sci. Bull.*, 2020, **65**, 272–275.
164 Y. Lin, M. I. Nugraha, Y. Firdaus, A. D. Scaccabarozzi, F. Aniés, A.-H. Emwas, E. Yengel, X. Zheng, J. Liu, W. Wahyudi, E. Yarali, H. Faber, O. M. Bakr, L. Tsetseris, M. Heeney and T. D. Anthopoulos, *ACS Energy Lett.*, 2020, **5**, 3663–3671.
165 P. Bi, S. Zhang, Z. Chen, Y. Xu, Y. Cui, T. Zhang, J. Ren, J. Qin, L. Hong, X. Hao and J. Hou, *Joule*, 2021, **5**, 2408–2419.
166 Z.-G. Zhang and Y. Li, *Angew. Chem., Int. Ed.*, 2021, **60**, 4422–4433.
167 H. Wang, H. Chen, W. Xie, H. Lai, T. Zhao, Y. Zhu, L. Chen, C. Ke, N. Zheng and F. He, *Adv. Funct. Mater.*, 2021, **31**, 2100877.
168 T. Wang, R. Sun, W. Wang, H. Li, Y. Wu and J. Min, *Chem. Mater.*, 2021, **33**, 761–773.
169 H. Yu, S. Luo, R. Sun, I. Angunawela, Z. Qi, Z. Peng, W. Zhou, H. Han, R. Wei, M. Pan, A. M. H. Cheung, D. Zhao, J. Zhang, H. Ade, J. Min and H. Yan, *Adv. Funct. Mater.*, 2021, **31**, 2100791.
170 H. Yang, H. Fan, Z. Wang, H. Yan, Y. Dong, C. Cui, H. Ade and Y. Li, *Macromolecules*, 2020, **53**, 9026–9033.
171 Z.-G. Zhang, Y. Yang, J. Yao, L. Xue, S. Chen, X. Li, W. Morrison, C. Yang and Y. Li, *Angew. Chem., Int. Ed.*, 2017, **56**, 13503–13507.
172 F. Peng, K. An, W. Zhong, Z. Li, L. Ying, N. Li, Z. Huang, C. Zhu, B. Fan, F. Huang and Y. Cao, *ACS Energy Lett.*, 2020, **5**, 3702–3707.
173 B. Liu, H. Sun, J.-W. Lee, J. Yang, J. Wang, Y. Li, B. Li, M. Xu, Q. Liao, W. Zhang, D. Han, L. Niu, H. Meng, B. J. Kim and X. Guo, *Energy Environ. Sci.*, 2021, **14**, 4499–4507.
174 Q. Fan, Q. An, Y. Lin, Y. Xia, Q. Li, M. Zhang, W. Su, W. Peng, C. Zhang, F. Liu, L. Hou, W. Zhu, D. Yu, M. Xiao, E. Moons, F. Zhang, T. D. Anthopoulos, O. Inganäs and E. Wang, *Energy Environ. Sci.*, 2020, **13**, 5017–5027.
175 A. Tang, J. Li, B. Zhang, J. Peng and E. Zhou, *ACS Macro Lett.*, 2020, **9**, 706–712.
176 Q. Fan, R. Ma, T. Liu, W. Su, W. Peng, M. Zhang, Z. Wang, X. Wen, Z. Cong, Z. Luo, L. Hou, F. Liu, W. Zhu, D. Yu, H. Yan and E. Wang, *Sol. RRL*, 2020, **4**, 2000142.
177 J. Du, K. Hu, L. Meng, I. Angunawela, J. Zhang, S. Qin, A. Liebman-Pelaez, C. Zhu, Z. Zhang, H. Ade and Y. Li, *Angew. Chem., Int. Ed.*, 2020, **59**, 15181–15185.
178 T. Jia, J. Zhang, W. Zhong, Y. Liang, K. Zhang, S. Dong, L. Ying, F. Liu, X. Wang, F. Huang and Y. Cao, *Nano Energy*, 2020, **72**, 104718.
179 S. Huang, F. Wu, Z. Liu, Y. Cui, L. Chen and Y. Chen, *J. Energy Chem.*, 2021, **53**, 63–68.
180 H. Yao, L.-K. Ma, H. Yu, J. Yu, P. C. Y. Chow, W. Xue, X. Zou, Y. Chen, J. Liang, L. Arunagiri, F. Gao, H. Sun, G. Zhang, W. Ma and H. Yan, *Adv. Energy Mater.*, 2020, **10**, 2001408.
181 Y. Li, Z. Jia, Q. Zhang, Z. Wu, H. Qin, J. Yang, S. Wen, H. Y. Woo, W. Ma, R. Yang and J. Yuan, *ACS Appl. Mater. Interfaces*, 2020, **12**, 33028–33038.
182 N. Chandrasekaran, E. Gann, N. Jain, A. Kumar, S. Gopinathan, A. Sadhanala, R. H. Friend, A. Kumar, C. R. McNeill and D. Kabra, *ACS Appl. Mater. Interfaces*, 2016, **8**, 20243–20250.
183 C. N. Hoth, S. A. Choulis, P. Schilinsky and C. J. Brabec, *J. Mater. Chem.*, 2009, **19**, 5398–5404.
184 M. Campoy-Quiles, Y. Kanai, A. El-Basaty, H. Sakai and H. Murata, *Org. Electron.*, 2009, **10**, 1120–1132.
185 M.-S. Kim, B.-G. Kim and J. Kim, *ACS Appl. Mater. Interfaces*, 2009, **1**, 1264–1269.
186 P. Cheng, G. Li, X. Zhan and Y. Yang, *Nat. Photonics*, 2018, **12**, 131–142.
187 R. Sun, W. Wang, H. Yu, Z. Chen, X. Xia, H. Shen, J. Guo, M. Shi, Y. Zheng, Y. Wu, W. Yang, T. Wang, Q. Wu, Y. Yang, X. Lu, J. Xia, C. J. Brabec, H. Yan, Y. Li and J. Min, *Joule*, 2021, **5**, 1548–1565.
188 Y. Kim, S. Cook, S. M. Tuladhar, S. A. Choulis, J. Nelson, J. R. Durrant, D. D. C. Bradley, M. Giles, I. McCulloch, C.-S. Ha and M. Ree, *Nat. Mater.*, 2006, **5**(3), 197–203.

